Cellulose (2024) 31:969–992
https://doi.org/10.1007/s10570-023-05569-y

ORIGINAL RESEARCH

Exploiting carboxymethyl cellulose-starch/alumina nano gel to eliminate Fe(III) from ore leachates of rare earth elements

G. A. Murad · G. A. Dakroury · E. M. Abu Elgoud

Received: 20 March 2023 / Accepted: 16 October 2023 / Published online: 8 November 2023

Abstract The present study describes the development of a novel nano gel of Carboxymethyl Cellulose Starch and Alumina (CMC-St/Al_2O_3) to purify the leach liquor of rare earth elements (REEs) minerals from Fe(III), which is considered the most contaminating metal in the REE liquor. CMC-St/Al_2O_3 nano gel was recognized by different analytical techniques such as FT-IR, SEM, TEM, X-ray diffraction, particle size, and thermal analysis. In a batch study, the best conditions for purifying REE from Fe(III) contaminants using CMC-St/Al_2O_3 nano gel were determined. For an initial concentration of 100 mg L^{-1}, 97.6% of Fe(III) was efficiently adsorbed onto CMC-St/Al_2O_3 after 15.0 min, pH = 2, and 25 °C. Due to the competition effect, the sorption efficiencies of the binary systems decreased to 68.4%, 72.97%, and 84.71% for the systems Fe(III)/La(III), Fe(III)/Sr(II), and Fe(III)/Cs(I), respectively. 99.9% of Fe(III) is eluted by 0.50 mol L^{-1} H_2SO_4. The sorption process was fitted with pseudo-second-order and the Langmuir model based on the error functions: Coefficient of determination (R^2), Reduced Chi-square (χ^2), The sum of square errors (SSE), and Corrected Akaike Information Criterion (AIC_c) as well as Residual error plots. The sorption process was spontaneous and exothermic. Finally, a CMC-St/Al_2O_3 nano gel was used to separate Fe(III) from the monazite liquor minerals and Sela leachate, mineralized from the Rosetta area and Gabal El Sela at Halaib environs, Egypt, with efficiencies of 89.03 and 92.7%, respectively.

Keywords Rare earth minerals · Extraction · Nano hydrogel · Fe(III) · Sorption

Introduction

The increasing demand for rare earth elements on the world market has led to the necessity of paying more attention to primary and secondary resources containing these elements (Buechler et al. 2019). Iron (III) is associated with the rare earth elements in several ores, especially those of the two much more common rare earth minerals, i.e., monazite and bastnaesite. Also, it is associated with spent nuclear fuels, which coexist with other metal ions, like heavy metal ions. This may be considered a restriction on the recovery and reuse of rare earth elements and heavy metals. The efficient separation of Fe(III) from rare earth elements

Supplementary Information The online version contains supplementary material available at https://doi.org/10.1007/s10570-023-05569-y.

G. A. Murad · E. M. Abu Elgoud
Nuclear Fuel Chemistry Department, Hot Laboratories Center, Egyptian Atomic Energy Authority, Cairo 13759, Egypt

G. A. Dakroury (✉)
Nuclear Chemistry Department, Hot Laboratories Centre, Egyptian Atomic Energy Authority, P.O. 13759, Cairo, Egypt
e-mail: dr_gdakrory2010@yahoo.com

represents a significant step change in the commercial production of these elements. As a result, the removal of Fe(III) from rare earth element solutions is critical (Abu Elgoud et al. 2022). Several techniques, such as ion exchange (Zhang et al. 2010), chemical oxidation, co-precipitation, electrochemical treatment, extraction (Abu Elgoud et al. 2020), membrane filtration (Soylak et al. 2010; Agboola et al. 2016; Noel Jacob et al. 2014), reverse osmosis, and adsorption, have been studied to remove heavy and precious metals from wastewater (Abu Elgoud et al. 2022; Shahr El-Din et al. 2021). Adsorption guarantees further development of its use in removing Fe(III) contaminants from liquors in the hydrometallurgical treatment of rare earth elements (Ang et al. 2018). Different adsorbents have been used for the removal of Fe(III). For example, Shahr El-Din et al. (2021) employed a calcium/alginate-graphene oxide (Ca/Alg–GO) nanocomposite for the removal of Fe(III), U(VI), and Th(IV) from rare earth chloride liquor. Their studies reported that the maximum sorption capacities of the Ca/Alg–GO nanocomposite for Fe(III), U(VI), and Th(IV) were approximately 139.0 mg g^{-1}, 129.0 mg g^{-1}, and 418.0 mg g^{-1}, respectively. The selective removal of Mn(II), Fe(III), and Ni(II) from Lanthanide solution by graphene oxide modified with sodium citrate (GO-C) has been investigated by Abu Elgoud et al. (2022). It was found that the GO-C composite shows high adsorption affinity towards Mn(II), Fe(III), and Ni(II) ions in the presence of lanthanides. Furthermore, the sorption isotherm data fit the Langmuir isotherm model with excellent adsorption capacities of 535.0, 223.22, and 174.65 mg g^{-1} for Fe(III), Mn(II), and Ni(II), respectively. The sorption of iron ions by graphene sheets has been studied by Change et al. (2013). They reported that the maximum sorption capacity of Fe(III) is 299.3 mg g^{-1}. Yuan et al. (2013) evaluated the behavior of poly(amidoamine) modified graphene oxide for the sorption of Cu(II), Zn(II), Fe(III), Pb(II), and Cr(III). Their work showed that the prepared poly (amidoamine) modified graphene oxide possessed maximum sorption capacities of 0.5312, 0.0798, 0.2024, 0.0513, and 0.1368 mmol g^{-1} for Fe(III), Cr(III), Zn(II), Pb(II), and Cu(II) ions, respectively. Additionally, the sorption of Fe(III), Zn(II), Pb(II), and Cd(II) has been studied using foam-infused GO by Lei et al. (2014).

The authors implied that the foam-infused GO possesses maximum adsorption capacities of 252.5, 381.3, 587.6, and 326 mg g^{-1} for Cd(II), Pb(II), Fe(III), and Zn(II), respectively. Abd-Elhamid and Aly (2018) employed thiosalcylic Acid for the removal of Fe(III) at pH 2.5. Their results demonstrated the maximum sorption capacity of Fe (III) was 275.78 mg g^{-1}. The removal of iron onto hazelnut hull from aqueous solutions has been examined by Sheibani et al. (2012). Their findings reported that the saturation sorption capacity of Fe(III) was 13.59 mg g^{-1}. Labib et al. (2020) prepared nano strontium cobaltite (SrCoOx) as an effective adsorbent for the purification of rare earth elements from monazite concentrate. The experimental result explored that the sorption efficiencies for Th(IV) and Fe(III) reach more than 99.0% without any noticeable sorption of rare earth elements. The sorption of iron and some lanthanides using aluminum silicotitanate have been investigated by Attallah et al. (2016). It was found that the sorption percentages of iron and some lanthanides were found to 79.0 and 99.0%, respectively. So it is confirmed that the prepared material is more effective for the recovery of lanthanide elements than Fe (III). Hamed et al. (2019) evaluated the sorption behavior of a novel polyaniline functionalized Tafa nanocomposite for U(VI), Th(IV), Ce(III), La(III), and Fe(III) from an aqueous solution. The results revealed that the prepared nanocomposite is extremely selective for Fe(III) ions higher than La(III), Ce(III), U(VI), and Th(IV) ions. The selective sorption of cerium and iron onto manganese-substituted cobalt ferrite nanoparticles has been examined by Hassan et al. (2022). Their results indicated that the maximum sorption capacities were found to be 130.0 and 161.0 mg g^{-1} for Ce(III) and Fe(III), respectively.

Superabsorbent hydrogels are unique materials that can absorb large amounts of water, typically more than 100 or even 1000 times their dry weight, resulting in significantly higher water content than regular hydrogels (Fekete et al. 2017). Carboxymethyl cellulose (CMC), a chemical derivative of cellulose, contains carboxylate and hydroxyl groups responsible for the strong interaction between CMC and Fe particles (Cao et al. 2011). Starch added to CMC systems improves their properties. Depending on the application, CMC/starch hydrogels may be a less expensive and more effective alternative to pure cellulose derivative-based gels (Fekete et al. 2017). The incorporation of inorganic nanomaterials in hydrogels could result in extra thermal stability and

an increase in surface area (Wahid et al. 2017). To the best of our knowledge, there is still no related report for CMC-starch nanomaterial hydrogel for adsorption applications.

The authors decided to use Al_2O_3 nanoparticles dispersed in super-adsorbent hydrogels of carboxymethyl cellulose and starch to separate Fe(III) from rare earth elements in ore leachate during this study. In addition, we investigated the selectivity of the prepared nano gel towards the sorption of iron ions under the best conditions in a binary system with Cs(I), Sr(II), and La(III). In the study's final section, the prepared adsorbent was used for iron recovery from the acidic liquor of monazite and Sela leachate.

Methodology

Reagents

Aluminum tri sec butylates, $C_{12}H_{27}AlO_3$ (purity ≥ 99%), and isopropyl alcohol, C_3H_8OH (purity ≥ 99.7%) were purchased from Merck, Germany, and used as precursors for Al_2O_3. Ammonium hydroxide NH_4OH (purity > 33%) from Adwic El-Nasr, Egypt. Sigma-Aldrich, USA, supplied starch. Sodium carboxymethyl cellulose (CMC) is from FoodChem Co., USA. The stock solution of 1000 mg/L Fe(III) was prepared using $FeCl_3.\ 4H_2O$ (purity ≥ 99.0%) obtained from Sigma-Aldrich was dissolved in minimum concentrated hydrochloric acid, evaporated to almost dryness, and then diluted to the desired concentration with double-distilled water. Ammonium thiocyanate (Alpha Chemika, India) Hydrochloric acid was obtained from Merck, NaOH (ADWIC), and Egypt. Monazite Liquor and Sela leachate were supplied by the nuclear materials authority; they were mineralized from the Rosetta area and Gabal El Sela at Halaib environs, Egypt, respectively.

Techniques of characterization

Using a Bomen Miclson FT-IR spectrophotometer, model MB157, Canada, the active functional groups of the nano gel were well identified.

Rigaku Goniometer MiniFlex 300/600 diffractometer, with 600 W X-ray tube D/teX Ultra2 silicon strip detector, air senestive ShapeFlex sample holder. $CuK_{\alpha 1}$ radiation (λ = 1.54060 Å) in 2θ ranging from 10° to 80° and step 0.01 was used to recognize the X-ray diffraction (XRD) pattern of Al_2O_3-NPs, CMC-St/Al_2O_3, and loaded CMC-St/Al_2O_3 powders with Fe(III). The scan rate was 2°/min, the operation voltage was 40 kV, and the current was 30 mA.

The thermal stability of the nano gel was evaluated using a thermal gravimetric analysis system of type DTA-TGA-50, Japan, at a constant rate of 5 °C/min from room temperature to 650 °C. The surface morphology of the prepared nano gel was investigated using a JEOL JSM-5400 scanning electron microscope from Japan with an accelerating voltage of 10.0 kV (SEM, FEI Quanta FEG-250, EDX). The samples were dried at 50 °C and coated with a layer of gold for conductivity purposes before imaging by the SEM apparatus. The high-resolution images of the samples investigated by transmission electron micrograph (TEM) images for particle size were recorded on a TEM, JEM2100, Jeol.s.b. Japan, with the highest accelerating voltage of 200 kV. The sample powders were milled very well and then dispersed for 10 min ultrasonically (Ultrasonic Cole-Parmer Instrument Company, Version Hills, Illinois 60,061, USA) in an ethanol solution. A drop from the suspension was then deposited on a Cu grid coated with a carbon film. The particle size of the prepared samples was determined using Zetasizer Nano-Zs, MALVERN, UK. The concentration of Fe(III) was measured by using the thiocyanate method (Marczenko 1986).

Preparation of CMC-St/Al_2O_3 nano gel

The steps for preparing nano-crystalline aluminum oxide using the sol–gel technique to hydrolyze aluminum tri sec butylate are summarised in Fig. 1. The prepared nano-aluminum oxide was used as filler in the CMC-St/Al_2O_3 nano gel. First, 2.0 g of Al_2O_3 nanoparticle (NP) was ultrasonically dispersed in 18.0 mL of distilled water acidified with 2.0 mL of 0.1 mol L^{-1} HCl for 30.0 min.

$$Al_2O_3 + 6HCl \rightarrow 2\ AlCl_3 + 3\ H_2O \quad (1)$$

The previous solution was then mixed with 30.0 mL of distilled water in a ratio of 1:1 starch: sodium carboxymethyl cellulose. A gel was successfully synthesized from low-concentration solutions at low pH (Fekete et al. 2017). Al^{3+} acts as a cross-linking agent, promoting gel formation by forming

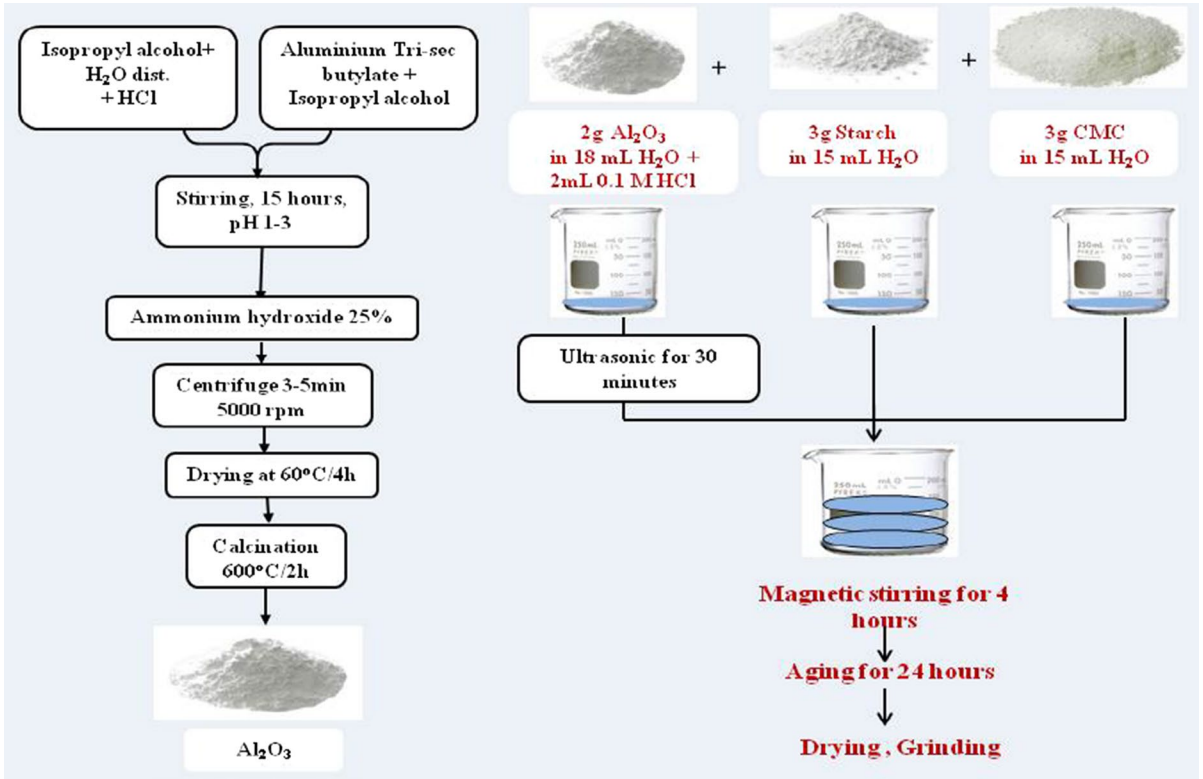

Fig. 1 Preparation steps for CMC-St/Al_2O_3 nano gel

a chemical bond with the negatively charged carboxymethyl groups of CMC (Zhang et al. 2022). The whole mixture was magnetically stirred for 4.0 h with a stirring rate of 100 rpm., and then the solution was aged in the mother solution for 24 h to achieve better homogeneity. The gelled mixture was dried for 48 h to constant weight before being grounded in an agate mortar to obtain a fine powder with a mesh size of less than 300 µm.

Sorption studies

The sorption attitudes of Fe(III) were investigated to optimize the separation conditions onto CMC-St/Al_2O_3 nano gel. 0.05 g of the nano gel was added to 25.0 mL glass bottles containing 5.0 mL of 100 mg $L.^{-1}$ Fe(III) aqueous solutions, and the resulting mixtures were shaken mechanically. pH, contact time, metal ion concentration, competing ions, and temperature were all studied according to this Table 1

The amount of Fe(III) sorption was calculated using Eqs. (2–4) (El-Shazly et al. 2022) as follows:

$$\text{Sorption efficiency}\,(\%) = \left(\frac{C_0 - C_e}{C_0}\right)100 \tag{2}$$

$$q_t = (C_O - C_t)\frac{V}{m} \tag{3}$$

$$q_e = (C_O - C_e)\frac{V}{m} \tag{4}$$

where q_e and q_t (mg g^{-1}) are the metal ion quantities sorbed on the sorbent at equilibrium and sorption time t (min), respectively. The initial metal ion concentration is C_o (mg L^{-1}), and the equilibrium metal ion concentration is C_e (mg L^{-1}). Furthermore, C_t represents the concentration of metal ions in the solution at time t, V denotes the volume (L) of the solution, and m denotes the weight of the adsorbent (g).

Kinetic and adsorption isotherm modeling

By evaluating the reaction's applicability for kinetic and isothermal adsorption modeling, the mechanism

Table 1 Experimental condition for sorption of Fe(III) onto CMC-St/Al_2O_3 nano gel

Effect of different parameters	pH	Contact time, min	[Fe(III)], mg/L	Adsorbent dosage, g	Temperature, K
Effect of solution pH	1,2,3,4, and 5	60.0	100.0	0.05	298
Effect of sorption time	2.0	1,3,5,15,30,60, and 120	100.0	0.05	298
Effect of iron concentration	2.0	15.0	100,200,400,600,800, and 1000	0.05	298
Effect of solution Temperature	2.0	15.0	100.0	0.05	298,308,318,328, and 338
Effect of adsorbent dosage	2.0	15.0	100.0	0.05,0.075, 0.1, 0.125, and 0.15	298

and potency of the sorption of Fe(III) onto CMC-St/Al_2O_3 nano gel could be largely decided. Adsorption isotherm modeling describes the interaction between the adsorbate particles and the surface of the adsorbent, whereas kinetic modeling describes the rate of the sorption reaction of the solute onto the adsorbate (Musah et al. 2022). Additionally, this modeling could be employed to clarify whether the sorption reaction is physisorption or chemisorption. To achieve these goals, the transient sorption data were subjected to four different types of kinetic modeling, including pseudo-1st order, pseudo- 2nd order, Elvoich, and intra-particle diffusion. As well as the Langmuir, Freundlich, Temkin, and Dubinin-Radushkevitch (D-R) models of adsorption isotherms. Tables 2 and 3 lists the non-linear form equations for the applied kinetic and adsorption isotherm modeling, respectively.

Error functions

The good fit is used to predict the best model by minimizing the error distribution between the experimental data and the predicted isotherm that best describes the interaction between the CMC-St/Al_2O_3 nano gel and Fe (III). Some of the error functions used to study model fit include Residual error plots (Chiachung 2014), Coefficient of correlation (R^2) (Ayawei et al. 2017), non-linear Chi-square test (Kumar and

Table 2 Non-linear form equation for the applied kinetic modeling

Model	Non-linear form	Description
Pseudo first order Dakroury et al. (2022a, b)	$q_{t=}q_{e(cal.)}\left(1-e^{-k_1 t}\right)$ (5)	Assume that adsorption is not influenced by adsorption in active sites. Instead, it might be a representation of external/internal diffusion. Wang and Guo (2020)
Pseudo-second order Dakroury et al. (2022a, b)	$q_t=\frac{k_2 q_{e(cal.)}^2 t}{1+k_2 q_e t}$ (6)	Assume that the adsorption occurs mainly on active sites Wang and Guo (2020)
Elvoich Khalil et al. (2022)	$q_t=\frac{1}{\beta}\ln(1+\alpha\beta t)$ (7)	It is widely used to describe adsorption processes with second-order kinetics. With the premise that the adsorbent's surface is energetically heterogeneous, they demonstrate evidence of chemisorption reactions. Ebelegi et al. (2020)
Intraparticle diffusion Dakroury et al. (2021)	$q_t=k_i t^{0.5}+C$ (8)	It describes the pure free diffusion of a solute in the pores or surface of a sorbent sphere. It does not facilitate by providing for the effect of adsorption Simonin and Bouté (2016)

q_e and q_t are the sorbed amounts of Fe(III) (mg g^{-1}) at equilibrium time and at any time t, respectively; k_1 (min^{-1}) is the pseudo 1st rate constant, k_2 (g mg^{-1} min^{-1}) is the pseudo 2nd order rate constant, α, β are the Elovich constants. α is the Elovich initial adsorption rate (mg g^{-1} min), β (g mg^{-1}) desorption constant

Table 3 Non-linear form equation for the applied isotherm modeling

Model	Non-linear form	Description
Langmuir Dakroury et al. (2022a, b)	$q_e = \frac{q_m K_L C_e}{1+K_L C_e}$ (9)	It implies that the adsorption occurs at specific homogeneous sites within an adsorbent with monolayer layer adsorption Musah et al. (2022)
Freundich Dakroury et al. (2022a, b)	$q_e = K_F C_e^{1/n}$ (10)	It describes the adsorption process on surface adsorption sites that are energetically heterogeneous with multilayer adsorption Musah et al. (2022)
Temkin Nebaghe et al. (2016)	$q_e = \frac{RT}{b_T \ln A_T C_e}$ (11)	Temkin isotherm model regarded the effects of indirect adsorbate/adsorbent interactions on the adsorption process; it is also assumed that the heat of adsorption (ΔH_{ads}) of all molecules in the layer decreases linearly as surface coverage increases Ayawei et al. (2017)
D-R Nebaghe et al. (2016)	$q_{mDR} = e^{-\beta_{DR}\varepsilon^2}$ (12)	D-R assumed the adsorption process was related to the micropore volume filling of heterogeneous adsorbent Hu, and Zhang (2019)

C_e is the concentration of Fe (III) at equilibrium. q_m is the monolayer sorption capacity (mg g^{-1}); K_L is constantly related to the free energy of adsorption (L mg^{-1}). K_f denotes for Freundlich constants and n denotes for sorption capacity and intensity. q_{mDR} is monolayer capacity For the D-R model, β_{DR} is a constant related to apparent adsorption energy, ε is Polanyi potential, R is the universal gas constant (8.314 JK^{-1} mol^{-1}), and T is the absolute temperature (K)

Porkodi 2007), Corrected Akaike information Criterion (AIC_c) (Moussa et al. 2023), and sum-of-squared errors (SSE) (Hamzah et al. 2018). The quantitative error function most commonly used during research is summarised in Table 4. Based on the definition of the error function, the best-fit adsorption isotherm will be minimized by either minimizing or maximizing the error functions. R^2 is the most commonly used error function for minimizing the error distribution between experimental equilibrium data and isotherms.

Thermodynamic parameters

Adsorption thermodynamics has an important role in estimating the nature of the sorption reaction. (Spontaneous or non-spontaneous). Three estimated thermodynamic parameters; the change in free energy (ΔG^o), the change in enthalpy (ΔH^o), and the change in entropy (ΔS^o); could be calculated by applying Eqs. (17–20) (Dakroury et al. 2022b; Abu Elgoud et al. 2023).

$$\Delta G^O = \Delta H - T\Delta S \tag{17}$$

$$\Delta G^O = -RT\ln K_d \tag{18}$$

$$\ln K_d = \frac{-\Delta H}{R} + \frac{\Delta S}{R}\cdot\frac{1}{T} \tag{19}$$

$$K_d = \frac{q_e}{C_e} \tag{20}$$

Table 4 Applied error function equations

Error function	Expression
Coefficient of determination (R^2) Kumar and Porkodi (2007)	$R^2 = 1 - \sum_{i=1}^{n}(q_{calc.} - q_{exp.})^2 / \sum_{i=1}^{n}(q_{calc.} - q_{mean})^2$ (13)
Reduced Chi-square (χ^2) Kumar and Porkodi (2007)	$\sum \frac{(q_{calc.} - q_{exp.})^2}{q_{calc.}}$ (14)
The sum of square Errors (SSE) Hamzah et al. (2018)	$\sum_{i=1}^{n}(q_{calc.} - q_{exp.})^2$ (15)
Corrected Akaike information Criterion (AIC_c) Moussa et al. (2023)	$AICc = (n\ln(SER/n)) + (2(p+1)) + (2(p+1)(p+2)/n - p - 2)$(16)

q_{exp} (mg g^{-1}) is the sorbed amount of Fe (III), $q_{calc.}$ (mg g^{-1}) is the predicted sorbed amount; q_{mean} (mg g^{-1}) is the mean of q_{exp} values of Fe (III), n is the experimental data points number, and p is the number of modelling parameters

ΔH^o and ΔS^o were determined from the slope and intercept obtained by plotting ln K_d against 1/T.

Desorption studies

Several eluting agents were used to investigate Fe(III) elution from loaded CMC-St/Al_2O_3 nano gel. After an hour, the mixture was filtered to separate the CMC-St/Al_2O_3 nano gel from the liquid phase, and the concentration of Fe(III) ions was determined. Equation (21) was used to compute desorption efficiency % (El-Shazly et al. 2022).

$$\text{Desorption}\% = \frac{C_{aq}}{C_s}\% \quad (21)$$

C_{aq} represents the concentration of Fe(III) in the aqueous phase, whereas C_s represents the concentration of Fe(III) within the CMC-St/Al_2O_3 nano gel.

Results and discussion

Sorbent characterization

FT-IR analysis

Figure 2a, b depicts the characteristic peaks of the nano gel. The carboxymethyl cellulose characteristic peaks were observed at 3423 cm^{-1} (broad absorption band due to stretching of –OH groups and intermolecular and intramolecular hydrogen bonds), 2926 cm^{-1} (C–H stretching), 1419 cm^{-1} (–CH_2 scissoring), 1320 cm^{-1} (–OH bending), and 1060 cm^{-1} (CHO–CH_2 stretching) (Bhandari et al. 2012). The peak at 1616 cm^{-1} confirmed cellulose carboxymethylation. At 1150–1100 cm^{-1}, the absorption band is represented by multiple peaks assigned to the C–O–C ether band. The main stretching vibration peaks of Al–O (Naayi et al. 2019) are at 856, 708, 654, 574, 528, 427, and 406 cm^{-1}. The intensities of the characteristic functional groups O–H broad band and ether bands from 1150 to 1023 cm^{-1} decreased after Fe (III) loading onto CMC-St/Al_2O_3 nano gel. This validates their contribution to the mechanism of the adsorption reaction.

Particle size and surface morphology

Figure 2c clarified the decrease in particle size for CMC-St/Al_2O_3 compared to Al_2O_3 NPs which was attributed to the reduction of the agglomeration of Al_2O_3 NPs by the dispersion in the hydrogel matrix (Gao et al. 2019). The average particle sizes of Al_2O_3 NP and CMC-St/Al_2O_3 were 79 nm and 51 nm, respectively. Furthermore, the decrease in the particle size of CMC-St/Al_2O_3 leads to a higher saturation surface concentration due to the increase in the number of active site densities (Wang and Shadman 2012). A rod-shaped, agglomerated, and uniform size for Al_2O_3 NP is illustrated by TEM with scale bar 50 nm in Fig. 2d, the nano-character of Al_2O_3 was investigated. The agglomerated spherical nanoparticles were due to the sol–gel preparation method.

Furthermore, Figs. 2e, f, and g with scale bars are 10 µm, 50 µm, and 10 µm respectively, represent SEM of the samples. SEM in Fig. 2e depicts Al_2O_3 particles rod-shaped, with particle sizes ranging from 13 to 30 nm and an average particle size of 22 nm. Figure 2f had a three-dimensional porous network structure due to Al^{3+} cross-linking the internal reactive groups with each other, causing macroscopically significant changes in the internal network structure of the CMC-St/Al_2O_3 nano gel. After Fe (III) loading in Fig. 2g, it was clarified that Fe (III) ions were trapped by the hydrophilic active sites in the empty spaces between gel folds (Hameed et al. 2020).

X-ray diffraction

The XRD patterns of Fe loaded onto CMC-St/Al_2O_3, CMC-St/Al_2O_3 nano gel, and Al_2O_3 nanoparticles were recorded at room temperature, as shown in Fig. 3a. The crystallographic planes highlight the crystalline structure of Al_2O_3-NPs. The XRD patterns indicate clearer and sharper peaks associated with alumina crystalline phases (Fig. 3b); α- Al_2O_3 ICDD ref. 00–005-0712, γ- Al_2O_3 ICDD ref. 00–010-0425, and θ- Al_2O_3 ICDD ref. 01-077-0396 (Lamouri et al. 2017; Sun et al. 2006; Feret et al. 2000; Karunakaran et al. 2011; Chauruka et al. 2015; Gheorghieș et al. 2009; Kim et al. 2012; Ansari and Husain 2011). Despite that, the line widths of peaks were broad in the case of CMC-St/Al_2O_3 and loaded CMC-St/Al_2O_3 with Fe (III) Fig. 3c, d, which revealed a smaller crystalline domain size. Also, the intensities for each peak

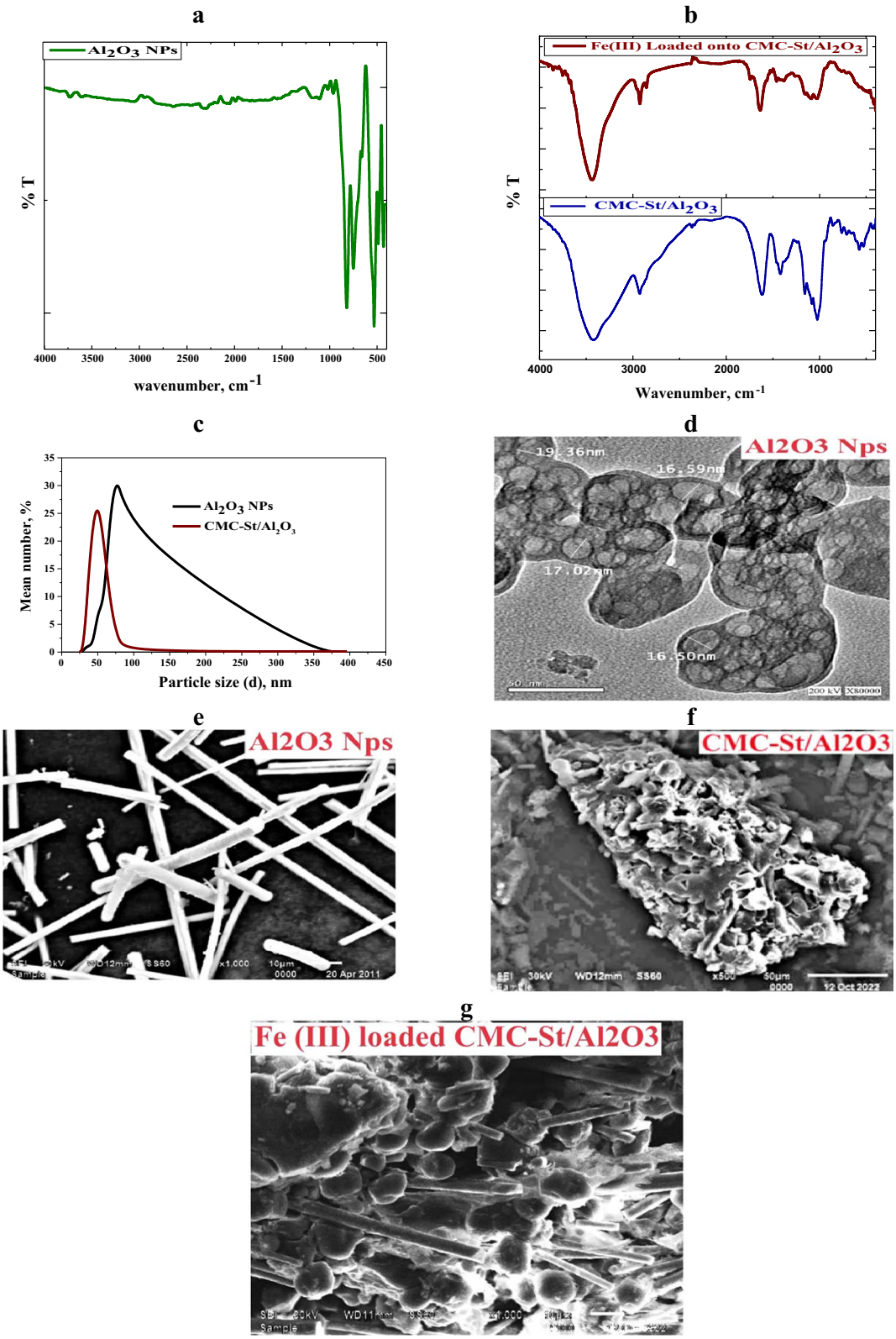
a
Al_2O_3 NPs
% T
wavenumber, cm^{-1}
b
Fe(III) Loaded onto CMC-St/Al_2O_3
CMC-St/Al_2O_3
% T
Wavenumber, cm^{-1}
c
Al_2O_3 NPs
CMC-St/Al_2O_3
Mean number, %
Particle size (d), nm
d
Al2O3 Nps
19.36nm
16.59nm
17.02nm
16.50nm
e
Al2O3 Nps
f
CMC-St/Al2O3
g
Fe (III) loaded CMC-St/Al2O3

◂**Fig. 2** **a** FTIR of Al_2O_3 NPs, **b** FTIR of CMC-St/Al_2O_3 nano gel and Fe- loaded CMC-St/Al_2O_3 nano gel **c-** Particle size distribution of AL_2O_3 and CMC-St/Al_2O_3 and **d** TEM of Al_2O_3 NPs **e** SEM of Al_2O_3 NPs, **f** SEM of CMC-St/Al_2O_3 nano gel, **g** Fe (III) loaded onto CMC-St/Al_2O_3 nano gel

were decreased in loaded CMC-St/Al_2O_3 with Fe(III) compared to CMC-St/Al_2O_3. It was further shown that the characteristic peaks of CMC-St/Al_2O_3 were shifted left when compared to Al_2O_3-NPs, whereas the peaks of loaded CMC-St/Al_2O_3 with Fe(III) were shifted back to the right of the original position. This demonstrates that the changes in the structure parameters occur on the surface of Al_2O_3-NPs as a result of the composition and the nature of the synthetic materials interphase. The particle size (D) of the crystallinity sample Al_2O_3-NPs was found to be 76 nm, which was determined using the formula of Scherrer Eq. (22).

$$D = \frac{k\lambda}{\beta\cos\theta} \tag{22}$$

where λ is the X-ray wavelength = 1.54060 Å, θ and β are the diffraction angle and the full width at half-maximum of the Al_2O_3 (222) line, respectively. *(k)* is the Scherrer constant of 0.9. However, the relative crystallinity of Al_2O_3, CMC-St/Al_2O_3, and loaded CMC-St/Al_2O_3 with Fe(III) was determined according to the relation (23)

$$\text{Relative crystallinity} = \frac{A_c}{A_c + A_a} \tag{23}$$

where A_c was the crystalline area and A_a was the amorphous area on the XRD spectra. The relative crystallinities of CMC-St/Al_2O_3 and loaded CMC-St/Al_2O_3 with Fe(III) are 45.1 and 37.5, respectively. This implies that sorption of Fe(III) notably degraded the crystalline region of Al_2O_3 NPs.

The particle size analyzed from the 222 line width of XRD peaks of the Al_2O_3 (Fig. 3a) was found to be 76 nm, in agreement with the previous measurement of Zetasizer in particle size and surface measurements in Sect. "Particle size and surface morphology". The X-ray pattern of CMC-St/Al_2O_3 nano gel significantly and substantially decreased the crystallinity.

Although pure CMC polymer is amorphous (Yao et al. 2020), the substitution of the hydroxyl group of CMC (Saadiah et al. 2019; Moussa et al. 2019) and the addition of 2 g nano Al_2O_3 could change the amorphous nature of CMC (Farrag et al. 2014). This confirms the formation of CMC-St/Al_2O_3 nano gel. For CMC-St/Al_2O_3 nano gel, at 16.9° and 20.22° are assigned for starch, while the amorphous maximum for loaded CMC-St/Al_2O_3 with Fe (III) appear at 24.55° and 19.47°. The aforementioned amorphous maximum indicate the presence of an A-typearrangement.

Thermal analysis

Figure 4a indicates the thermal stability of nano Al_2O_3 with a total weight loss of 18.75% up to 600 °C. An endothermic peak was found at 71.98 °C with accompanying weight loss of 7.6% due to the evaporation of physically adsorbed and structured water. An exothermic peak at 220 °C and a broad one at 539 °C with a total weight loss of 11.15% due to organic by-product combustion and phase transformation (Zuo et al. 2016). The first endothermic peak of the CMC-St/Al_2O_3 nano gel shifted to 150 °C with a weight loss of 8.93%, indicating that the CMC-St/Al_2O_3 possesses relatively higher thermal stability, as shown in Fig. 4b, with two exothermic peaks at 311 °C and 505 °C and a total weight loss of 54.6% due to organic material degradation.

Sorption studies

Effect of pH

The choice of pH for the sorption reaction is the most important study in the optimization of the sorption parameters. As the pH controls the surface charge of the sorbent, the solubility of the adsorbate, and the $[H^+]$ concentration on the sorbent functional groups. Figure 5a depicts the effect of pH on the sorbed amount of Fe^{3+} onto CMC-St/Al_2O_3 nano gel within the pH range (0.5 to 2.5). The Fe(III) sorbed amount increased from 4.24 mg g^{-1} to 9.99 mg g^{-1} as the pH was raised from 0.5 to 2.5 due to the decrease in $[H^+]$ concentration around the composite surface and the less competition between Fe(III) and H^+ ions for the occupancy of available active sites. Furthermore, Fig. 5b shows Fe(III) speciation along pH 1–14, which was studied by Hydra/Medusa chemical equilibrium software (Puigdomenech 2013). Fe(III) was the dominant species till pH 2. As the pH was

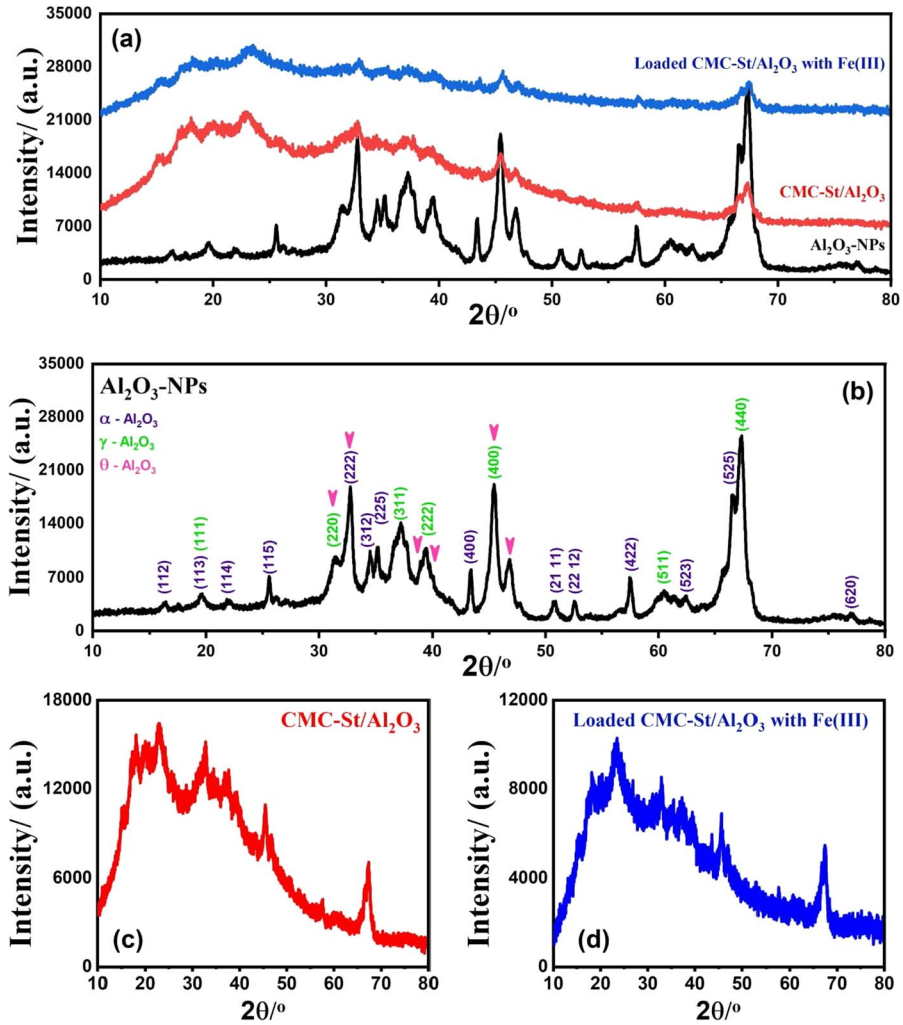

Fig. 3 XRD of a- Al_2O_3 NPs, CMC-St/Al_2O_3, and Fe(III) loaded onto CMC-St/Al_2O_3 nano gel Al_2O_3 NPs, b- Al_2O_3 NPs, c- CMC-St/Al_2O_3, d- Fe(III) loaded onto CMC-St/Al_2O_3 nano gel was recorded at room temperature

raised above 2, the solubility of Fe(III) decreased, and Fe(III) hydroxy complexes (Fe $(OH)^{2+}$, (Fe $(OH)_2{}^{+}$, and Fe_2 $(OH)_2{}^{4+}$) started to appear till pH 4. At pH > 4, Fe $(OH)_3$ was the dominant species (Sheibani et al. 2012). The chemical stability of CMC-St/Al_2O_3 nano gel was studied (Fig. 5c) and showed that CMC-St/Al_2O_3 nano gel is stable in an acidic medium, and stability reached 97.5% at pH = 2. The CMC-St/Al_2O_3 nano gel found in suspension in a 0.5 mol L^{-1} NaCl solution exhibited a point of zero charges (pH_{pzc}) at pH 1.755 (Fig. 5d). At pH values greater than the pH_{pzc} value, the surface of the hybrid nano-composites became negative, which facilitated the adsorption of Fe(III) ions (Râpă et al. 2021).The working pH was chosen to be 2.0 to avoid precipitation and hydroxyl complexes. Examining the sorption efficiency of CMC-St/Al_2O_3 nano gel towards rare earth ions taking La(III) as an example, it was depicted that the nano gel has no affinity towards La(III) as a result of the competing protons in this range, and REE adsorption via ion exchange processes onto the nano gel was not favorable at this pH range of 0.5–2.5 (Ramasamy et al. 2019).

Effect of time

Figure 6a depicts the effect of conducting time on the sorption of Fe(III) onto CMC-St/Al_2O_3 nano gel at pH 2, V/m ratio 0.1, temperature 25 °C, and an initial concentration of Fe(III) of 100 mg L^{-1}. The sorption reaction occurred, and the amount of Fe (III) sorbed increased rapidly until the

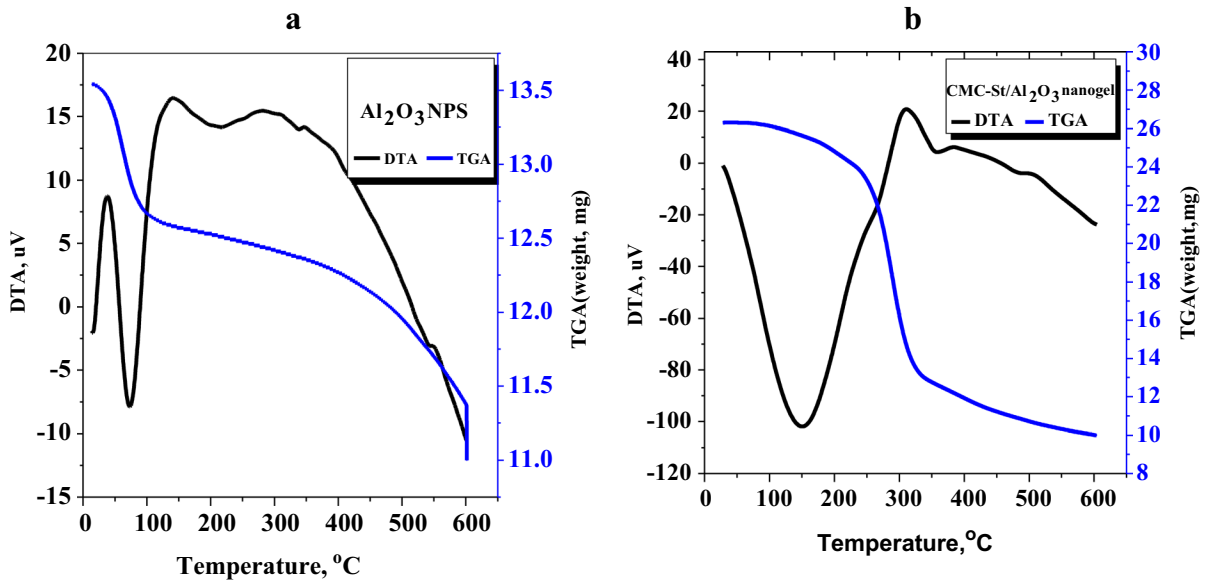

Fig. 4 TGA-DTA of **a** AL_2O_3 NPs, **b** CMC-St/Al_2O_3 nano gel

equilibrium time of 20.0 min. This was due to the availability of free active sites on the surface of the CMC-St/Al_2O_3 nano gel during the early stages of the sorption process and the gradual occupancy of these sites until equilibrium caused a decrease in the sorption rate (Khalil et al. 2022). As the time increased from 1.0 to 15.0 min, the sorbed amount increased from 7.423 mg g^{-1} to 9.985 mg g^{-1}.

Effect of metal ion concentration

As shown in Fig. 6b, the rate of Fe (III) sorption onto CMC-St/Al_2O_3 nano gel at pH 2, V/m ratio 0.1, temperature 25 °C, and equilibrium time 15.0 min depends on the concentration of Fe(III) in the range (100–1000 mg L^{-1}). The sorption rate decreased as the Fe(III) concentration increased due to a limited number of available free active sites (Alghamdi et al. 2019) particularly in comparison to an increase in the number of Fe(III) at the CMC-St/Al_2O_3 nano gel surface (Igberase et al. 2017). From an initial concentration of 100 mg L^{-1} of Fe(III) to an initial concentration of 1000 mg L^{-1}, the sorbed efficiency of Fe(III) onto CMC-St/Al_2O_3 nano gel slipped from 96.48% to 29.08%.

Effect of V/m ratio

To determine the volume-mass ratio effect on the sorption process at pH 2, initial concentration of Fe(III) 100 mg L^{-1}, temperature 25 °C, and equilibrium time 15.0 min, 5.0 mL of Fe (III) is contacted with different masses (0.15–0.1 g) of CMC-St/Al_2O_3 nano gel (Fig. 6c). The sorbed amount of Fe (III) increased as the V/m ratio increased. This means that as sorbent mass increases, sorption efficiency increases because the number of free active sites on the CMC-St/Al_2O_3 nano gel increases for the same Fe(III) concentration (Igberase and Osifo 2015).

Effect of temperature

Figure 6d illustrates the effect of temperature on the sorption reaction at pH 2, V/m ratio 0.1, initial concentration of Fe(III) 100 mg L^{-1}, and equilibrium time 15.0 min. The rate of sorption decreased from 96.48% to 67.25% as the temperature increased from 25.0 to 65.0 oC due to the decrease in surface activity. These findings explained the exothermic nature of Fe (III) sorption onto CMC-St/Al_2O_3 nano gel.

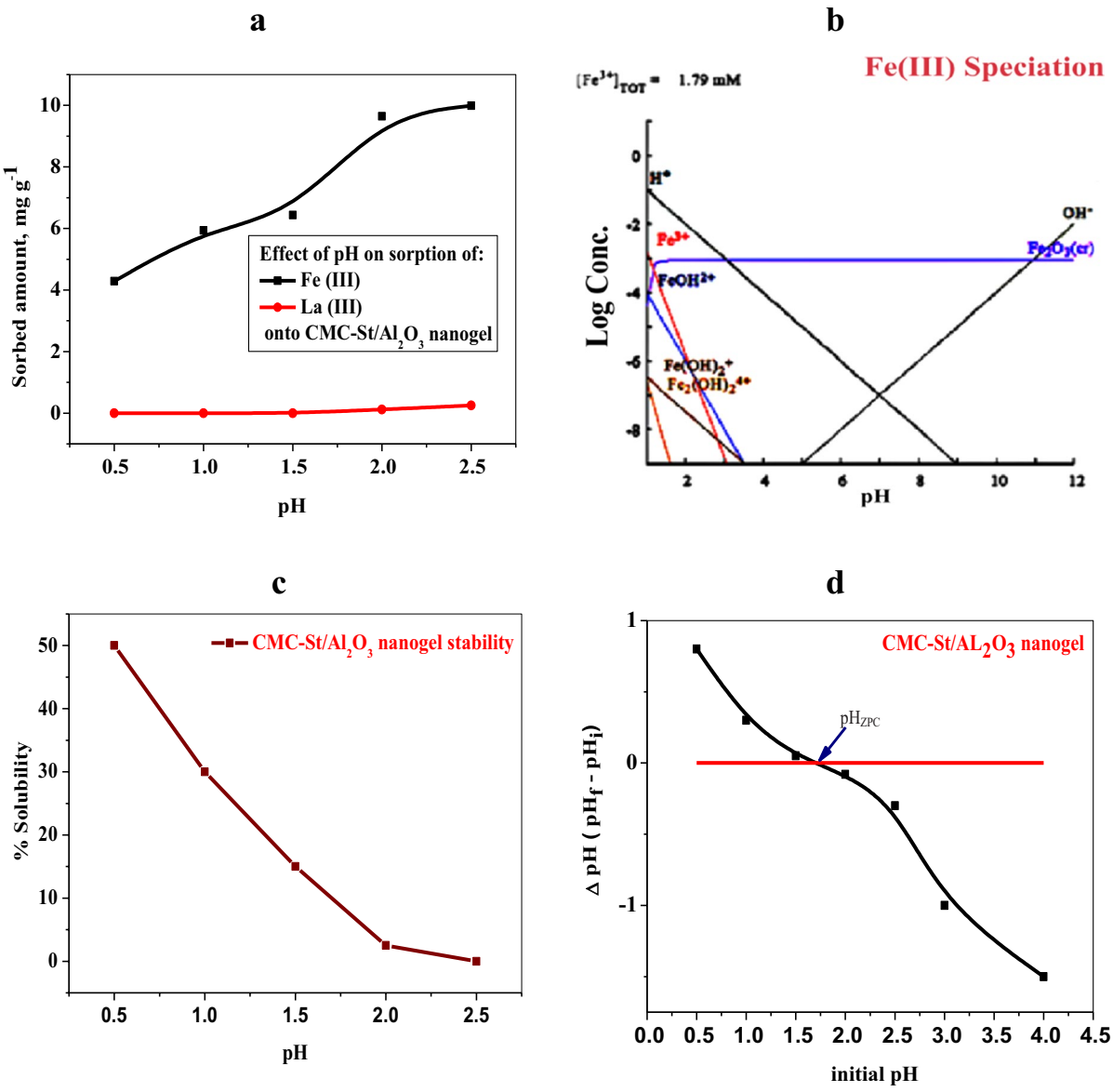

Fig. 5 **a** The influence of pH on the sorbed amount of Fe^{3+} onto CMC-St/Al_2O_3 nano gel. **b** Speciation diagram of Fe (III), **c** The chemical stability CMC-St/Al_2O_3 nano gel at different pH of HCl acid, and **d** pH_{ZPC} of CMC-St/Al_2O_3 nano gel. [C_i = 100 mg L^{-1}, Contact time = 60 min., V/m = 0.1 L $g.^{-1}$, Temp. = 25 °C]

Binary system and multi-component system

Figure 7a depicts how the sorption efficiency of Fe(III) was affected by the presence of competing ions Cs(I), Sr(II), and La(III) in a binary system. It decreased from about 97.6% to 84.71% in the presence of 100 mg L^{-1} of Cs(I), while decreasing from 97.6% to 72.97% in the presence of 100 mg L^{-1} Sr(II). However, La(III) had the highest competing effect, and sorption efficiency reached 68.12%. This behavior could be explained in terms of radius ions and electronegativity. The ions with a smaller ionic radius and high electronegativity would have a high sorption capacity (Goel et al. 2004). Thus, the sorption efficiency decreased in the order La(III) > Sr(II) > Cs(I). Although CMC-St/Al_2O_3 nano gel had no sorption

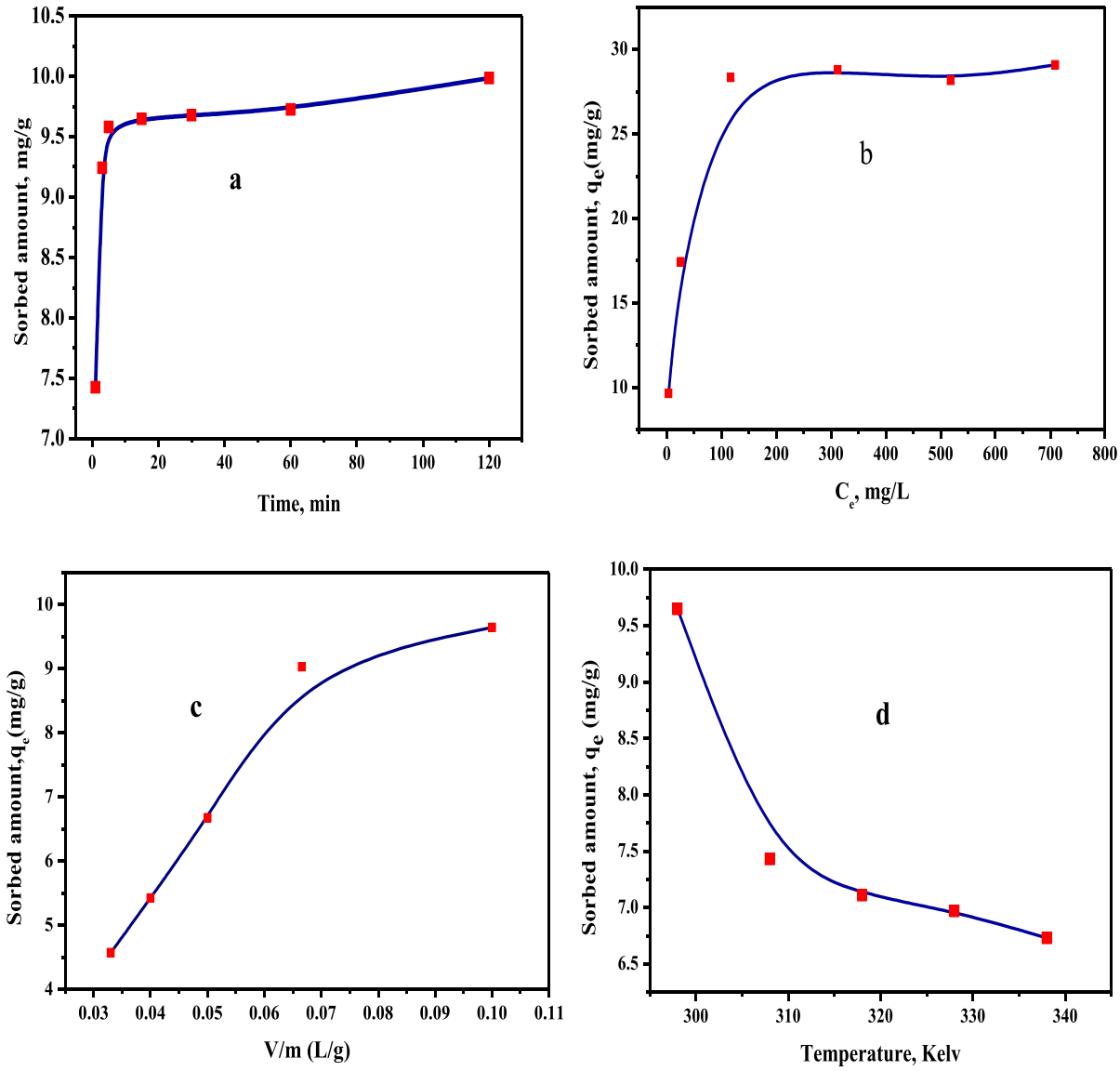

Fig. 6 The effect of: a- Time b- concentration c- V/m ratio d- Temperature on the sorbed amount of Fe^{3+} onto CMC-St/Al_2O_3 nano gel

affinity towards La(III) in a single system, the presence of La(III) hinders the sorption process of Fe(III). This could be explained in terms of the hydration sphere as the smaller size of metal ions have higher hydration tendencies in addition to fewer tendencies to lose water in the hydration sphere (Cristiani et al. 2021). This hinders Fe (III) from joining the active sites.

For the multi-component system of Fe(III), La(III), Cd(II), and Cs(I), 2.5 mL of 100 mg L^{-1} for each was mixed and conducted with 0.2 g of CMC-St/Al_2O_3 nano gel at pH 2 for 15.0 min at 25 °C. The sorption efficiency of Fe (III) decreased more than that in the single system due to competing effects, from 97.6% to 90.1%. Furthermore, the sorption efficiency of La (III) increased in the multi-component system compared to that in the single system, attributed to the synergetic effects between sorbates and CMC-St/Al_2O_3 nano gel did not reach equilibrium (Barros et al. 2019). Figure 7b shows the sorption efficiency of Fe(III), La(III), Cd(II), and Cs(I). The rate of sorption of the elements had the order Fe(III) > La(III) >

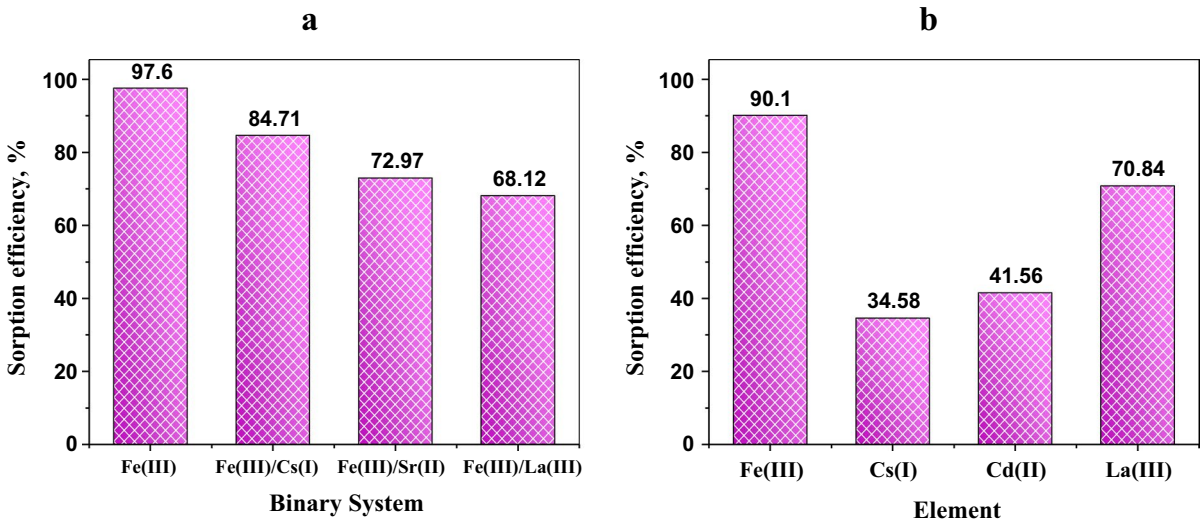

Fig. 7 The sorption efficiency of CMC-St/Al_2O_3 nano gel towards Fe(III) a- In the binary system **b** In the multi-component system. [Eq. Time = 15.0 min, C_i, = 100 mg L^{-1}, pH = 2, Temp. = 25 °C, V/m = 0.1 L $g.^{-1}$]

Table 5 Ionic radius, electronegativity, and charge density of Cs(I), Sr(II), La(III), and Fe(III)

Ion	Ionic radius (A^o)	Electronegativity	Charge density Z/r
Cs(I)	1.69	0.79	0.592
Sr(II)	1.13	0.95	1.769
Cd(II)	0.97	1.69	2.062
La(III)	1.06	1.1	2.832
Fe(III)	0.65	1.83	4.615

Cd(II) > Cs(I) in agreement with the charge density order in Table 5.

Kinetic modeling

Figure 8a illustrates the non–linear fitting of the kinetic modeling. The error functions of the applied kinetic model fitting were present in Table 6; it was determined that the sorption of Fe (III) onto CMC-St/Al_2O_3 nano gel was regulated by a pseudo-2nd order mechanism based on R^2 (0.948), the highest value among all the applied models and the lowest values of χ^2, SSE, and AIK_c. In terms of residual error for the qualitative error function in Fig. 8b, the pseudo-2nd order model produced relatively low error residuals. As a result, the best-fit model of Fe(III) sorption onto CMC-St/Al_2O_3 nano gel was the pseudo-2nd order model, and a chemisorption mechanism for the reaction was recommended. Furthermore, the calculated ($q_{t,\ calc.}$) value was close to the experimental equilibrium adsorption capacity ($q_{t,\ exp.}$)

Adsorption isotherm

Figure 8c shows the applied isotherm model fitting along with its associated parameters and quantitative error functions, which are listed in Table 7. The highest R^2 (0.929), lowest $\chi 2$, SSE, and AIK_c (0.0015, 0.00603, and −35.398, respectively) found in the estimated error-function of Langmuir model fitting that recommended it as the best suitable mechanism for the sorption reaction.

Furthermore, the residual error of the fitting isotherm model in Fig. 8d revealed that Langmuir has relatively low error residuals. The monolayer capacity of CMC-St/Al_2O_3 towards Fe(III) was 0.524 mmol g^{-1} (29.26 mg g^{-1}). Based on the R_L values, the sorption reaction is favorable because ($0 < R_L < 1$).

Thermodynamic studies

The standard free energy change (ΔG^o) values for the sorption of Fe(III) ions on CMC-St/Al_2O_3 nano

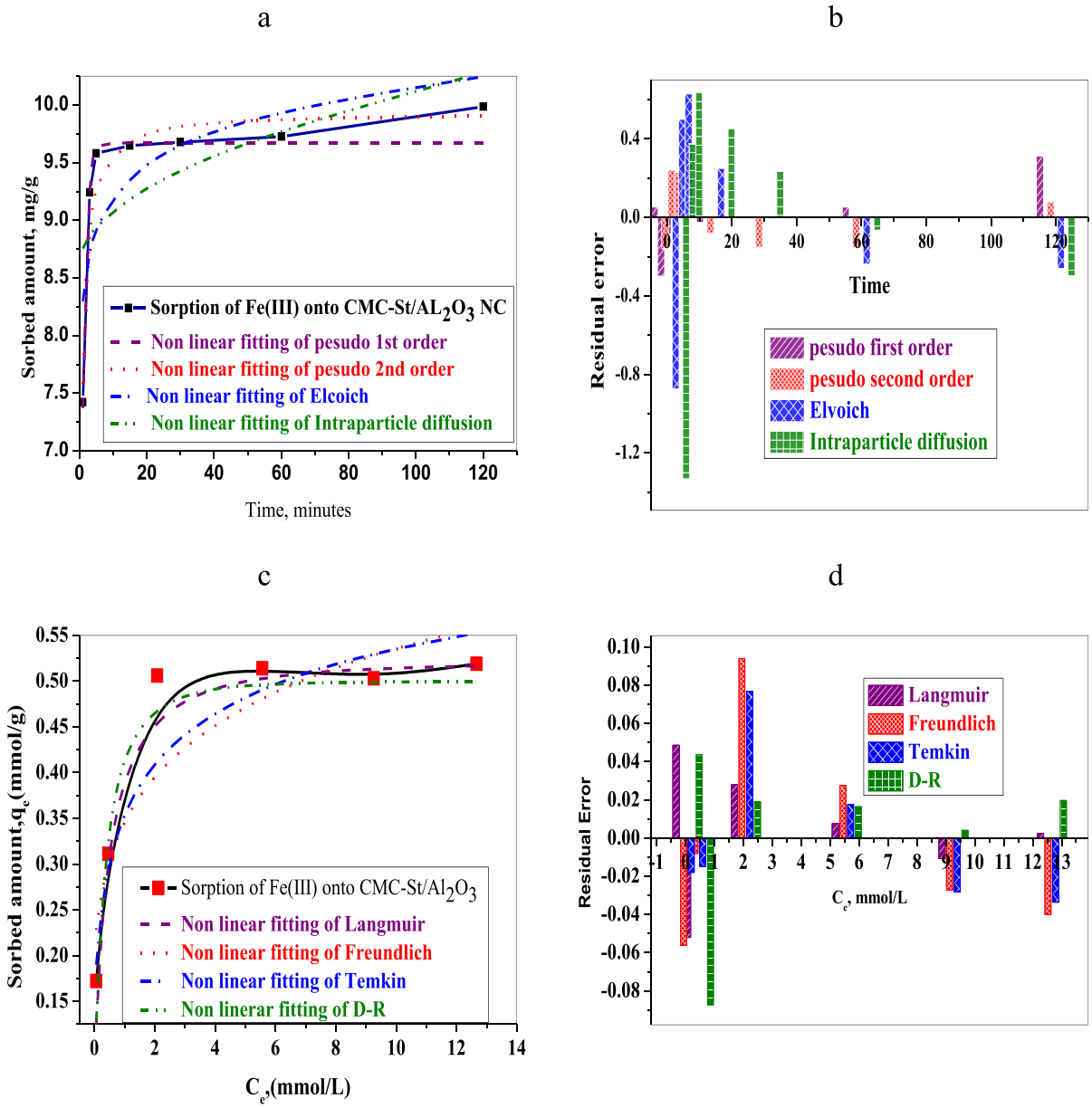

Fig. 8 Non-linear fitting of **a** the kinetic models, **c** the isotherm models and Residual errors of **b** the kinetic models, **d** of the isotherm models studied for the sorption of Fe(III) onto CMC-St/Al_2O_3

gel were calculated using Eq. 23, while the standard enthalpy (ΔH^o) and standard entropy changes (ΔS^o) were calculated using the slope and intercept of the line plotted using Eq. 21 in Fig. 9, and they are shown in Table 8. The measured adsorption enthalpy is (-9.544 kJ mol^{-1}) pointing to an exothermic process. A high equilibrium constant was attained if the ΔG^o value was negative (Yeddou and Bensmaili 2007). The affinity of CMC-St/Al_2O_3 nano gel to adsorb Fe(III) is indicated by the positively sign of ΔS^o ($+15.985$ J mol^{-1}) in this Eq. (18).

Table 6 Estimated coefficients and error-function data for kinetic modeling applied for the sorption of Fe(III) ONTO CMC-St/Al_2O_3

Parameters	Kinetic model
Pseudo-1st-order	
q_t (mg g^{-1}) (calculated)	9.674
K_1 (min^{-1})	1.435
R^2	0.947
χ^2	0.0401
SSE	0.2003
AIC_c	− 10.877
Pseudo-2nd-order	
q_t (mg g^{-1}) (calculated)	9.932
K_2 (g mg^{-1} min^{-1})	0.325
R^2	*0.948*
χ^2	*0.0393*
SSE	*0.1963*
AIC_c	*− 11.018*
q_t (mg g^{-1}) (experiment)	**9.985**
Elovich kinetic model	
α (mg g^{-1} min^{-1})	2.917
β (g mg^{-1})	2.46
R^2	0.576
χ^2	0.319
SEE	1.595
AIC_c	3.647
Intra-particle diffusion model	
K	0.15339
C	8.603
R^2	0.289
χ^2	0.543
SEE	2.673
AIC_c	7.261

The highest R^2 and the lowest χ2, SSE, and AIC_c are in bold and Italics

Table 7 Estimated coefficients and error function data for adsorption isotherm models applied for the sorption of Fe(III) ONTO CMC-St/Al_2O_3

Parameters	Adsorption isotherm models
Langmuir model	
q_{mL}	0.525
K_L	4.875
R_L	0.281
R^2	*0.929*
χ^2	*0.0015*
SSE	*0.00603*
AIC_c	*− 35.398*
Freundlich model	
N	5.92
K_f (mmol $^{n-1}$ $g^{-1}.L^{-n}$)	0.364
R^2	0.822
χ^2	0.0038
SSE	0.0151
AIC_c	**− 28.972**
Temkin model	
K	255.496
B	0.0684
R^2	0.898
χ^2	0.00217
SSE	0.00867
AIC_c	− 32.857
Dubinin-Radushkevich model	
q_{mDR} (mol g^{-1})	0.4999
β_{DR} ($mmol^2$ kJ^{-2})	0.1702×10^{-8}
E (kJ mol^{-1})	8.168
R^2	0.876
χ^2	0.0093
SSE	0.01054
AIC_c	− 31.489

The highest R^2 and the lowest χ2, SSE, and AIC_c are in bold and Italics

Desorption process

To minimize the need for a constant supply of adsorbent and decrease overall waste, a desorption process is essential. Therefore, the process is more effective, and the sorbent is better with a higher desorption percentage (Ossian et al. 2014). The desorption efficiencies using HNO_3, H_2SO_4, and HCl were investigated in Fig. 10. The sorbed Fe(III) had desorption efficiencies in the order of $HCl > H_2SO_4 > HNO_3$ for a 0.1 mol L^{-1} concentration, concerning the K_a acids strengths for HCl, H_2SO_4, and HNO_3: 1.3×10^6, 1×10^3, and 2.4×10, respectively. For both H_2SO_4 and HNO_3, the desorption efficiencies increased to 99% as the acid concentration was increased to 0.5 mol L^{-1}. For the desorption process, 0.5 mol L^{-1} H_2SO_4 is chosen for economic consideration. Due to the chemical stability of CMC-St/Al_2O_3 nano gel in Sect. "Effect of pH", where more than 50% of CMC-St/Al_2O_3 nano gel was degraded at pH less than 0.5. So, CMC-St/

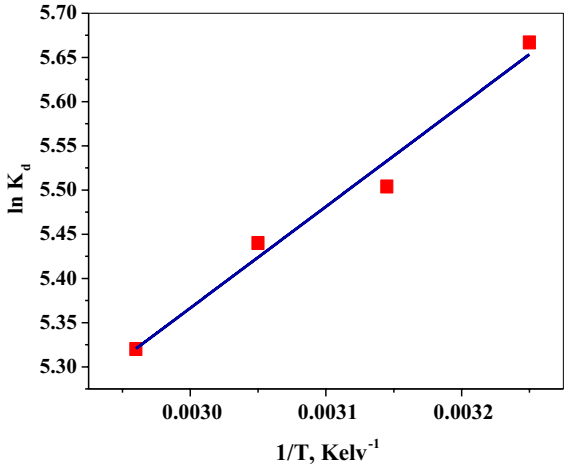

Fig. 9 Thermodynamic plot for Fe(III) sorption onto CMC-St/Al_2O_3 nano gel

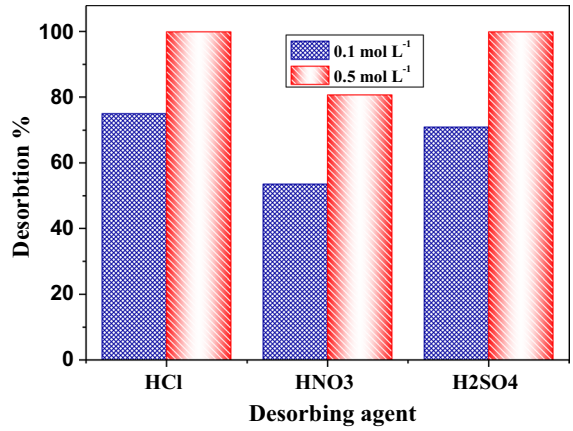

Fig. 10 Desorption efficiency of Fe(III) sorbed onto CMC-St/Al_2O_3 nano gel using different eluents with different concentration at 25 °C

Al_2O_3 has a drawback for the regeneration process, but according to the cost of its constituent, it could be recommended as a sorbent for Fe(III). Fe(III) was separated from Al_2O_3 in the desorbed solution by magnetic seeding separation (Han et al. 2021).

Mechanism discussion

Figure 11 suggests a possible mechanism for the preparation of CMC-St/Al_2O_3 nano gel where Al^{3+} is formed by Eq. 1. Three CMC molecules are linked to Al^{3+} form cross-linked $(CMC)_3$-Al then starch is linked to the OH-group of CMC. This mechanism was suggested by Braihi (2014). Regarding the FT-IR spectrum of CMC-St/Al_2O_3 nano gel in Fig. 2b, The intensities of the peaks for the O–H group and the ether group C–O–C decreased after Fe(III) loading. This supports the possibility that these groups could contribute the sorption reaction. This is due to the lowest space hindrance at this site. So, the sorption mechanism of Fe(III) onto CMC-St/Al_2O_3 nano gel takes place through three routes: (i) movement of Fe(III) from the solution bulk to the CMC-St/Al_2O_3 nano gel surface. (ii) Diffusion of Fe(III) from the boundary layer inside the pores of CMC-St/Al_2O_3 nano gel. (iii) Sorption of Fe(III) onto the active functional groups mentioned through electrostatic attraction force. The following chemical equations (Eqs. 24, 25) propose a mechanism for Fe(III) sorption onto CMC-St/Al_2O_3 nano gel.

$$3\ \mathrm{CMC-St/Al_2O_3-OH} + \mathrm{Fe^{3+}} \rightarrow \left(\mathrm{CMC-St/Al_2O_3-O}\right)_3-\mathrm{Fe} + 3\ \mathrm{H^+} \quad (24)$$

$$3\ \mathrm{CMC-St/Al_2O_3-O-} + \mathrm{Fe^{3+}} \rightarrow \left(\mathrm{CMC-St/Al_2O_3-O}\right)_3-\mathrm{Fe} \quad (25)$$

Real application

The efficiency of Fe(III) separation onto CMC-St/Al_2O_3 nano gel from rare earth mineral leachate was examined using digested Monazite concentrate by

Table 8 Thermodynamic parameters for **Fe(III)** sorption onto CMC-St/Al_2O_3 nano gel

Sorbent	Δ H° kJ mol^{-1}	ΔS° J mol^{-1} K^{-1}	ΔG° kJ mol^{-1}			
			Temperature (K)			
			298	308	318	328
CMC-St/Al_2O_3	− 9.544	15.985	− 14.31	− 14.47	− 14.63	− 14.79

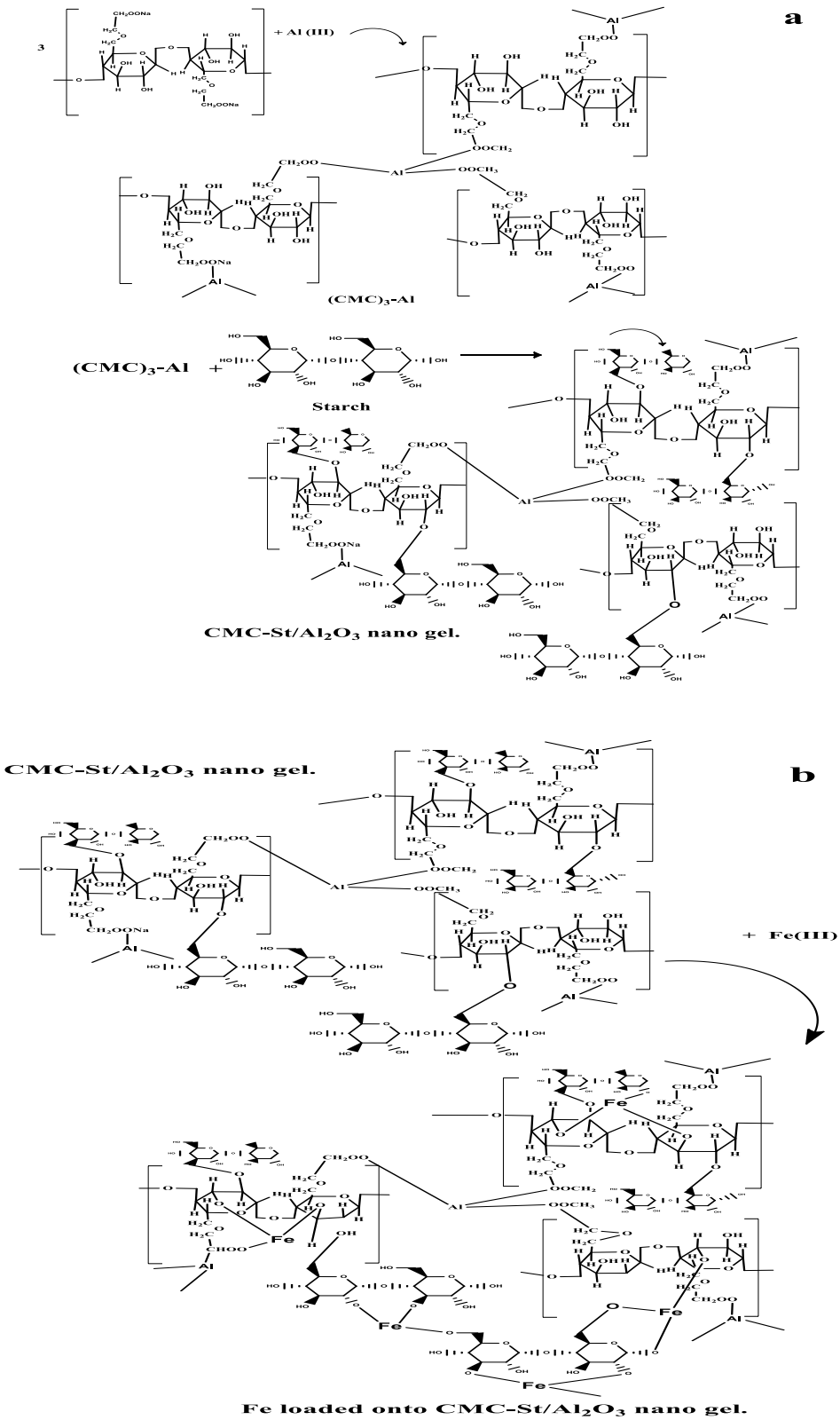
a
+ Al (III)
(CMC)3-Al
(CMC)3-Al +
Starch
CMC-St/Al2O3 nano gel.
b
CMC-St/Al2O3 nano gel.
+ Fe(III)
Fe loaded onto CMC-St/Al2O3 nano gel.

◂**Fig. 11** Suggested mechanism for a- CMC-St/Al_2O_3 nano gel preparation and b- sorption of Fe(III) onto CMC-St/Al_2O_3 nano gel

caustic soda (Ali et al. 2022) and sulfate leaching solutions of Sela mineralization (Khawassek et al. 2015) with initial concentrations of total rare earth of 25,000 mg g^{-1} and 3481 mg g^{-1}, respectively. 0.1 g of CMC-St/Al_2O_3 nano gel was conducted with 10 mL of the digested rare earth minerals solutions at the optimum sorption parameters (pH = 2, equilibrium time = 15.0 min at 25 °C). The initial and final solution concentrations of rare earth elements and Fe(III) were measured. The sorption efficiency of Fe(III) and total rare earth in the monazite liquor and Sela leachate is listed in Table 9. The distribution coefficient and separation factor were calculated using Eqs. (26), and (27).

$$K_d(ml/g) = \left(\frac{C_i - C_f}{C_f}\right) \times \frac{V}{m} \quad (26)$$

$$SF_{\frac{Fe}{REE}} = \frac{K_d(Fe)}{K_d(REE)} \quad (27)$$

The higher separation factor for Fe(III) and rare earth elements in the case of monazite liquor than Sela leachate was due to the higher percentage of rare earth elements in monazite liquor than Sela leachate. Figure 12a, b indicated the SEM of loaded CMC-St/Al_2O_3 nano gel monazite liquor and Sela leachate onto CMC-St/Al_2O_3 nano gel. Comparing them with the SEM of CMC-St/Al_2O_3 nano gel (Fig. 2f,), the monazite liquor and Sela leachate onto the CMC-St/Al_2O_3 nano gel image depicted a rougher and denser structure due to the occupation of Fe (III) ions and traces of rare earth elements, as indicated in EDX results (Fig. 12 c, d). The main peaks for C, O, and Al are referred to as the main constituents of CMC-St/Al_2O_3 nano gel while Fe(III) and some rare earth elements confirm the sorption and separation processes. The appearance of the S peak in the EDX spectrum of Sela leachate is due to H_2SO_4 used in the digestion process of Sela ores. All of the absorption peaks observed in the IR spectra of loaded CMC-St/Al_2O_3 nano gel with Monazite liquor and Sela leachate (Fig. 12 e, f) were also present in the IR spectra of pure CMC-St/Al_2O_3 nano gel. However, the intensity of the carboxyl absorption peaks decreased due to the adsorption of Fe(III) and trace amounts of rare earth elements. A great similarity between Fig. 2b for the IR spectra of Fe-loaded onto CMC-St/Al_2O_3 nano gel and Fig. 12 e, f of loaded monazite liquor and Sela leachate onto CMC-St/Al_2O_3 nano gel confirms the participation of carboxyl functional and ether groups in the sorption process. The result indicated the possibility of using CMC-St/Al_2O_3 nano gel, as a prospective material, to separate Fe(III) from REEs in the rare ore leachates, especially for monazite liquor.

Conclusion

A new nano gel Carboxymethyl cellulose-Starch/Alumina (CMC-St/Al_2O_3) was successfully prepared with an average particle size of 51 nm by the sol–gel technique. The prepared nano gel was characterized to investigate its structure and functional groups using FT-IR, SEM, TEM, X-ray diffraction, Particle size, and thermal analysis. The investigation clarified the nanostructure of the prepared nano hydrogel with modifications in thermal stability. Sorption experiments were carried out to estimate the possibility of its use to purify the leach liquor of rare earth minerals from Fe(III), which is considered the most contaminating metal in the REE mineral liquor. 97.6% of Fe(III) efficiently sorbed onto CMC-St/Al_2O_3 at pH = 2, after 15.0 min, at an initial concentration of 100 mg L^{-1} and 25 °C. The sorption efficiency decreased to 68.4% in the binary system of Fe(III)/La(III), 72.97% for Fe(III)/Sr(II), and 84.71% for the

Table 9 Sorption efficiency and separation of Fe (III) from rare earth minerals leachate onto CMC-St/Al_2O_3 nano gel

Rare earth mineral leachate	Sorption efficiency (%)		Distribution coefficient k_d		Separation factor
	Fe (III)	Total rare earth	Fe (III)	Total rare earth	
Monazite liquor	89.03	5	923.5	5.263	175.47
Sela Leachate	92.7	14.84	36.990	17.426	2.122

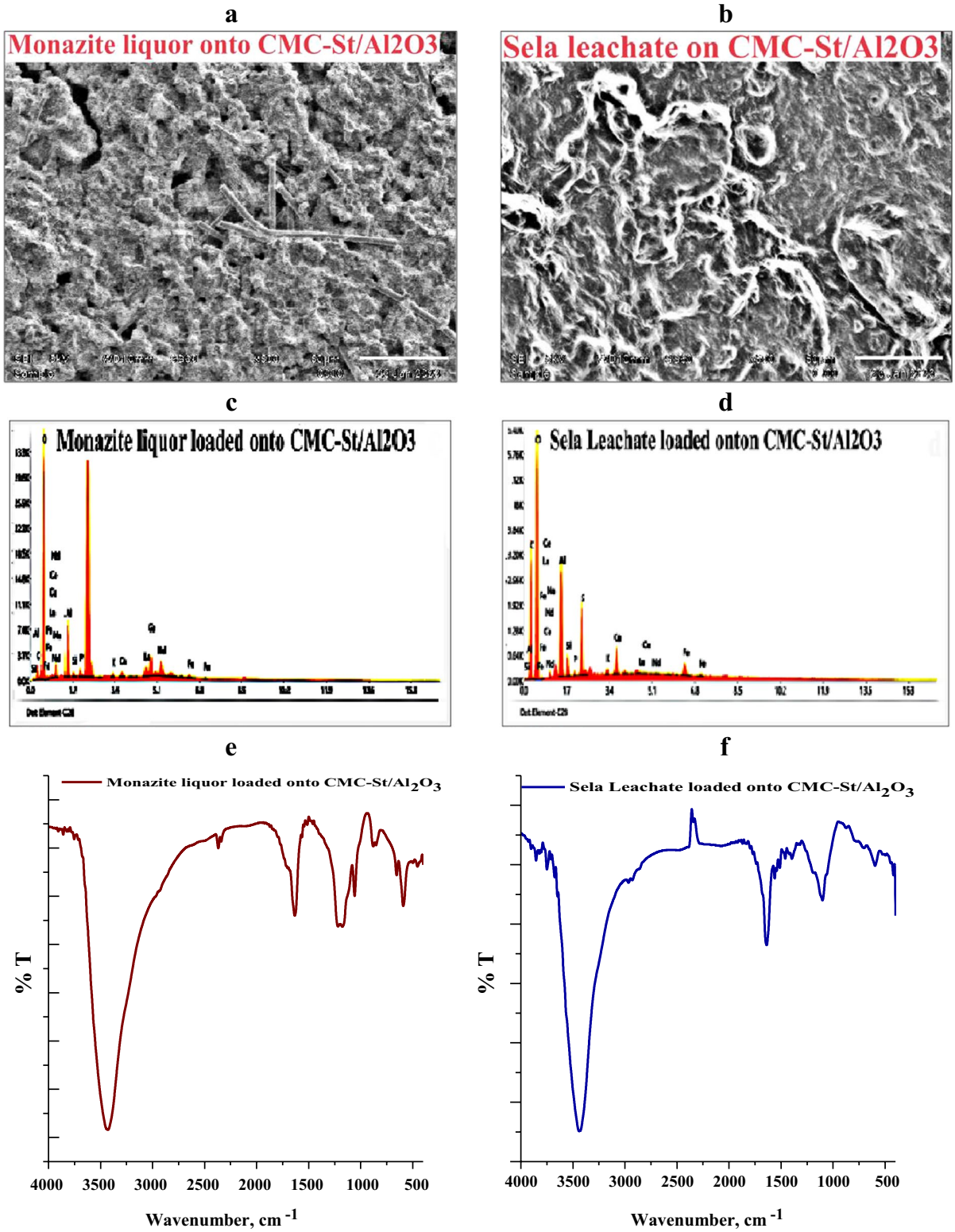

Fig. 12 **a, b** SEM, **c, d** EDX and **e, f** FTIR of loaded monazite liquor and Sela Leachate sorbed onto CMC-St/Al_2O_3 nano gel, respectively

Fe(III)/Cs(I) binary system due to the competition effect. 99.9% of Fe(III) eluted by 0.5 mol L^{-1} H_2SO_4. The sorption process was fitted with a pseudo-2nd-order and Langmuir model based on the error functions: Coefficient of determination (R^2), Reduced Chi-square (χ^2), Sum of square Errors (SSE), and Corrected Akaike Information Criterion (AIC_c) as well as residual error plots. The sorption process was spontaneous and exothermic. Finally, (CMC-St/Al_2O_3) nano gel was used to adsorb Fe(III) from the minerals liquor Monazite and Sela at the optimized sorption condition with sorption efficiency of 89.03% and 92.7%, respectively.

Acknowledgments The authors thank all the staff members and colleagues of Hot Laboratories Centre of Egyptian Atomic Energy Authority for their cooperation and useful help offered during this work. A lot of thanks to Assoc. Prof. A.A. Eliwa and Dr. Sh.M. Abdo, Nuclear material Authority for their cooperation for the real application section.

Author contributions All authors contributed to the study conception and design, Material preparation, data collection and analysis. All authors read and approved the final manuscript.

Funding Open access funding provided by The Science, Technology & Innovation Funding Authority (STDF) in cooperation with The Egyptian Knowledge Bank (EKB). The authors received no financial support for the research, authorship, and/or publication of this article.

Data availability All the data used for this work are publicly available.

Declarations

Conflict of interest The authors declare that they have no conflict of interest.

Ethical approval The authors confirm that the manuscript has been read and is approved by all authors. The authors declare that this manuscript has not been published and not under consideration for publication elsewhere**.**

Consent to participate All of the authors consented to participate in the drafting of this manuscript.

Consent for publication All of the authors consent to publish this manuscript.

Research involving human participants or animals Not applicable.

References

Abd-Elhamid AI, Aly HF (2018) Removal of Fe (III) from aqueous solution using thiosalcylic acid as an efficient and novel adsorbent. Egypt J Chem 61(4):617–627. https://doi.org/10.21608/EJCHEM.2018.3312.1280

Abu Elgoud EM, Ismail ZH, El-Nadi YA, Aly HF (2020) Separation of cerium (IV) and yttrium (III) from citrate medium by solvent extraction using D2EHPA in kerosene. Chem Pap 74(8):2461–2469. https://doi.org/10.1007/s11696-020-01083-8

Abu Elgoud EM, Abd-Elhamid AI, Emam S, Aly HF (2022) Selective removal of some heavy metals from Lanthanide solution by graphene oxide functionalized with sodium citrate. Sci Rep 12(1):1–13. https://doi.org/10.1038/-022-17949-8

Abu Elgoud EM, Abd-Elhamid AI, Aly HF (2023) Modification of graphene oxide with imidazolium-based ionic liquid for significant sorption of (III) and Pr (III) from s41598aqueous solutions. Appl Water Sci La 13(7):152. https://doi.org/10.1007/s13201-023-01955-w

Agboola O, Mokrani T, Sadiku R (2016) Porous and fractal analysis on the permeability of nanofiltration membranes for the removal of metal ions. J Mater Sci 51:2499–2511. https://doi.org/10.1007/s10853-015-9562-3

Alghamdi A, Al-Odayni A, Saeed W, Al Kahtani A, Alharthi F, Aouak T (2019) Efficient adsorption of lead (II) from aqueous phase solutions using polypyrrole-based activated carbon. Materials. https://doi.org/10.3390/ma12122020

Ali AH, Dakroury GA, Hagag MS, Abdo ShM, Allan KF (2022) Sorption of some rare earth elements from acidic solution onto poly(acrylic acid–co-acrylamide/16, 16-dimethylheptadecan-1-amine) composite. J Polym Environ 30:1170–1188. https://doi.org/10.1007/s10924-021-02271-7

Ang KL, Li D, Nikoloski AN (2018) The effectiveness of ion exchange resins in separating uranium and thorium from rare earth elements in acidic aqueous sulfate media. Part 2. Chelating Resins Minerals Eng 123:8–15. https://doi.org/10.1016/j.mineng.2018.04.017

Ansari SA, Husain Q (2011) Immobilization of Kluyveromyces lactis β galactosidase on concanavalin A layered aluminium oxide nanoparticles—Its future aspects in biosensor applications. J Mol Catal B Enzym 70(3–4):119–126

Attallah MF, Elgazzar AH, Borai EH, El-Tabl AS (2016) Preparation and characterization of aluminum silicotitante: ion exchange behavior for some lanthanides and iron. J Chem Technol Biotechnol 91:2243–2252. https://doi.org/10.1002/jctp.4810

Ayawei N, Ebelegi AN, Wankasi D (2017) Modelling and interpretation of adsorption isotherms. J Chem. https://doi.org/10.1155/2017/3039817

Barros Ó, Costa L, Costa F, Lago A, Rocha V, Vipotnik Z, Silva B, Tavares T (2019) Recovery of rare earth elements from wastewater towards a circular economy. Molecules 24(6):1005. https://doi.org/10.3390/molecules24061005

Bhandari PN, Jones DD, Hanna MA (2012) Carboxymethylation of cellulose using reactive extrusion. Carbohydr Polymer 87:2246–2254. https://doi.org/10.1016/j.carbpol.2011.10.056

Braihi A (2014) Proposed cross-linking model for carboxymethyl cellulose/starch superabsorbent polymer blend. Int J Mater Sci Appl 3:363. https://doi.org/10.11648/j.ijmsa.20140306.23

Buechler DT, Zyaykina NN, Spencer CA, Lawson E, Ploss NM, Hua I (2019) Comprehensive elemental analysis of consumer electronic devices: rare earth, precious, and critical elements. Waste Manag 103:67–75. https://doi.org/10.1016/j.wasman.2019.12.014

Cao J, Xu C, Tang H, Tang S, Cao M (2011) Synthesis of monodispersed CMC-stabilized Fe-Cu bimetal nanoparticles for in situ reductive dechlorination of 1, 2, 4 trichlorobenzene. Sci Total Environ 409:2336–2341. https://doi.org/10.1016/j.scitotenv.2011.02.045

Chang CF, Truong QD, Chen JR (2013) Graphene sheets synthesized by ionic-liquid assisted electrolysis for application in water purification. Appl Surf Sci 264:329–334. https://doi.org/10.1016/j.apsusc.2012.10.022

Chauruka SR, Hassanpour A, Brydson R, Roberts KJ, Ghadiri M, Stitt H (2015) Effect of mill type on the size reduction and phase transformation of gamma alumina. Chem Eng Sci 134:774–783

Chiachung C (2014) Evaluation of equilibrium sorption isotherm equations. Open Chem Eng J 7:24–44. https://doi.org/10.2174/1874123101307010024

Cristiani C, Bellotto M, Dotelli G, Latorrata S, Ramis G, Gallo Stampino P, Zubiani EMI, Finocchio E (2021) Rare earths (La, Y, and Nd) adsorption behaviour towards mineral clays and organoclays: monoionic and trionic solutions. Minerals 11(1):30. https://doi.org/10.3390/min11010030

Dakroury GA, Ali SM, Hassan HS (2021) Assessment of adsorption performance of chitosan/ZrO2 biosorbent composite towards Cs (I) and Co (II) metal ions from aqueous solution. J Polym Res 28:385. https://doi.org/10.1007/s10965-021-02753-1

Dakroury GA, El-Shazly EAA, Eliwa AA, Mubark AE, El-Azony KM (2022a) Utilization of titanium nanocomposites as prospective materials for recycling of vanadium (V) from waste solutions. J Mol Liq 366:120170. https://doi.org/10.1016/j.molliq.2022.120170

Dakroury GA, El-Shazly EAA, Hassan HS (2022b) Sorption of lead (II) and strontium (II) ions from aqueous solutions onto non-living Chlorella Vulgaris Alga/Date pit activated carbon composite. Carbon Lett 32:495–512. https://doi.org/10.1007/s42823-021-00280-z

Ebelegi AN, Ayawei N, Wankasi D (2020) Interpretation of adsorption thermodynamics and kinetics. Open J Phys Chem 10:166–182. https://doi.org/10.4236/ojpc.2020.103010

El-Shazly EAA, Moussa SI, Dakroury GA (2022) Recovery of some rare-earth elements by sorption technique onto graphene oxide. J Sustain Metall 8:715–731. https://doi.org/10.1007/s40831-022-00520-0

Farrag A, Ali H, Atta A, Balboul M (2014) Influence of nanostructured TiO2 additives on some physical characteristics of carboxymethyl cellulose (CMC). J Radiat Res Appl Sci 7:36–43. https://doi.org/10.1016/j.jrras.2013.11.004

Fekete T, Borsa J, Takács E, Wojnárovits L (2017) Synthesis of carboxymethylcellulose/starch superabsorbent hydrogels by gamma-irradiation. Chem Central J. https://doi.org/10.1186/s13065-017-0273-5

Feret FR, Roy D, Boulanger C (2000) Determination of alpha and beta alumina in ceramic alumina by X-ray diffraction. Spectrochim Acta, Part B 55(7):1051–1061

Gao H, Zhang M, Yang H, Li Z, Li Y, Chen L (2019) A novel green synthesis of γ-Al2O3 nanoparticles using soluble starch. Mod Phys Lett B 33(16):1950182. https://doi.org/10.1142/s0217984919501823

Gheorghieș C, Gheorghieș L, Ciortan S, Păunoiu V, Cantaragiu A, Lalău C, Rusu DE (2009) Structural analysis of alumina thin layer prepared by controlled oxidation process. Annals of" Dunarea de Jos" University of Galati. Fascicle v, Technol Machine Build 27:319–322

Goel J, Kadirvelu K, Rajagopal C (2004) Competitive sorption of Cu(II), Pb(II) and Hg(II) ions from aqueous solution using coconut shell-based activated carbon. Adsorpt Sci Technol 22(3):257–273. https://doi.org/10.1260/0263617041503453

Hamed MM, Shahr El-Din AM, Abdel-Galil EA (2019) Nanocomposite of polyaniline functionalized Tafla: synthesis, characterization, and application as a novel sorbent for selective removal of Fe (III). J Radioanal Nucl Chem 322(2):663–676. https://doi.org/10.1007/s10967-019-06733-0

Hameed A, Khurshid S, Adnan A (2020) Synthesis and characterization of carboxymethyl cellulose based hydrogel and its applications on water treatment. Desalin Water Treat 195:214–227. https://doi.org/10.5004/dwt.2020.26041

Hamzah S, Razali NS, Yatim NI, Alias M, Ali A, Zaini NS, Azzam AAM (2018) Characterisation and performance of thermally treated rice husk as efficient adsorbent for phosphate removal. J Water Supp Res and Tech-Aqua 67(8):766–778. https://doi.org/10.2166/aqua.2018.087

Han H, Wenjuan S, Wei S et al (2021) Magnetic separation of impurities from hydrometallurgy solutions and waste water using magnetic iron ore seeding iron ores. IntechOpen. https://doi.org/10.5772/intechopen.93728

Hassan MR, Shahr El-Din AM, Aly MI (2022) Selective recovery of cerium (III) and iron (III) from nitrate medium by manganese substituted cobalt ferrite magnetic nanoparticles as low cost synthesized sorbent. Int J Environ Anal Chem. https://doi.org/10.1080/03067319.2022.2038144

Hu Q, Zhang Z (2019) Application of Dubinin-Radushkevich isotherm model at the solid/solution interface: a

theoretical analysis. J Mol Liq. https://doi.org/10.1016/j.molliq.2019.01.005
Igberase E, Osifo P (2015) Equilibrium, kinetic, thermodynamic and desorption studies of cadmium and lead by polyaniline grafted cross-linked chitosan beads from aqueous solution. J Ind Eng Chem 26:340–347. https://doi.org/10.1016/j.jiec.2014.12.007
Igberase E, Osifo P, Ofomaja A (2017) The adsorption of Pb, Zn, Cu, Ni, and Cd by modified ligand in a single component aqueous solution: equilibrium, kinetic, thermodynamic, and desorption studies. Int J Anal Chem 2017:15. https://doi.org/10.1155/2017/6150209
Karunakaran C, Anilkumar P, Gomathisankar P (2011) Photoproduction of iodine with nanoparticulate semiconductors and insulators. Chem Cent J 5(1):1–9
Khalil M, Dakroury GAS, Borai EH (2022) Efficient sorption and group separation of rare earth elements using modified CuO nanocomposite. Surfaces Interfaces 33:102233. https://doi.org/10.1016/j.surfin.2022.102233
Khawassek M, Eliwa AA, E.A. Gawad EA, Abdo SM, (2015) Recovery of rare earth elements from El-Sela effluent solutions. J Radiat Res Appl Sci 8(4):583–589. https://doi.org/10.1016/j.jrras.2015.07.002
Kim HS, Park NK, Lee TJ, Um MH, Kang M (2012) Preparation of nanosized α-A l 2 O 3 particles using a microwave pretreatment at mild temperature. Adv Mater Sci Eng. https://doi.org/10.1155/2012/920105
Kumar KV, Porkodi K (2007) Mass transfer, kinetics and equilibrium studies for the biosorption of methylene blue using Paspalum notatum. J Hazard Mater 146:214–226. https://doi.org/10.1016/j.jhazmat.2006.12.010
Labib S, Shahr El-Din AM, Allan KF, Attallah MF (2020) Synthesis of highly deficient nano SrCoOx for the purification of lanthanides from monazite concentrate. J Radioanal Nucl Chem 323(3):1179–1188. https://doi.org/10.1007/s10967-020-07031-w
Lamouri S, Hamidouche M, Bouaouadja N, Belhouchet H, Garnier V, Fantozzi G, Trelkat JF (2017) Control of the γ-alumina to α-alumina phase transformation for an optimized alumina densification. Boletín De La Sociedad Española De Cerámica y Vidrio 56(2):47–54
Lei Y, Luo Y, Zhang L (2014) Synthesis of three-dimensional graphene oxide foam for the removal of heavy metal ions. Chem Phys Lett 593:122–127. https://doi.org/10.1016/j.cplett.2013.12.066
Marczenko Z (1986) Spectrophotometric determination of elements. Wiley, New York
Moussa I, Khiari R, Moussa A, Belgacem N, Mhenni MF (2019) Preparation and characterization of carboxymethyl cellulose with a high degree of substitution from agricultural wastes. Fibers Polym 20:933–943. https://doi.org/10.1007/s12221-019-8665-x
Moussa SI, Mekawy ZA, Dakroury GA et al (2023) Linear and non linear recognition for the sorption of 60Co and 152+154Eu radionuclides onto Bio CuO nanocomposite. J Polym Environ 31:2148–2165. https://doi.org/10.1007/s10924-022-02735-4
Musah M, Azeh Y, Mathew J, Umar Tanko M, Abdulhamid Z, Muhammad A (2022) Adsorption kinetics and isotherm models: a review. Caliphate J Sci Technol. https://doi.org/10.4314/cajost.v4i1.3
Naayi S, Hassan A, Salim E (2018) FTIR and X-ray diffraction analysis of Al2O3 nanostructured thin film prepared at low temperature using spray pyrolysis method. Int J Nanoelectron Mater 11:1–6
Nebaghe KC, El Boundati Y, Ziat K, Naji A, Rghioui L, Saidi M (2016) Comparison of linear and non-linear method for determination of optimum equilibrium isotherm for adsorption of copper(II) onto treated Martil sand. Fluid Phase Equilib 430:188–194. https://doi.org/10.1016/j.fluid.2016.10.003
Noel Jacob K, Senthil Kumar S, Thanigaivelan A, Tarun M, Mohan D (2014) Sulfonated polyethersulfone-based membranes for metal ion removal via a hybrid process. J Mater Sci 49:114–122
Osiane P, Li PW, Gjergj DKO, Toyohisa F, Kohei M, Takafumi A, Gouki S, Masayoshi N (2014) Recovery of rare earth elements from aqueous solution obtained from Vietnamese clay minerals using dried and carbonized parachlorella. J Environ Chem Eng 2:1070–1081. https://doi.org/10.1016/j.jece.2014.04.002
Puigdomenech I (2013) Make equilibrium diagrams using sophisticated algorithms (MEDUSA). Inorganic Chemistry. Royal institute of technology, Stockholm Sweden. http://www.kemi.kth.se/medusa. https://sites.google.com/site/chemdiagr/
Ramasamy DL, Puhakka V, Doshi B, Iftekhar S, Sillanpää M (2019) Fabrication of carbon nanotubes reinforced silica composites with improved rare earth elements adsorption performance. Chem Eng J 365:291–304. https://doi.org/10.1016/j.cej.2019.02.057
Râpă M, Ţurcanu AA, Matei E, Predescu AM, Pantilimon MC, Coman G, Predescu C (2021) Adsorption of copper (II) from aqueous solutions with alginate/clay hybrid materials. Mater (basel, Switzerland) 14(23):7187. https://doi.org/10.3390/ma14237187
Saadiah MA, Zhang D, Nagao Y, Muzakir SK, Samsudin AS (2019) Reducing crystallinity on thin film based CMC/PVA hybrid polymer for application as a host in polymer electrolytes. J Non-Cryst Solids 511:201–211
Shahr El-Din AM, Monir T, Borai EH (2021) Graphene oxide caged biopolymer nanocomposite for purification of rare earth elements from high grade egyptian monazite concentrate. J Polym Environ 29(11):3721–3731. https://doi.org/10.1007/s10924-021-02146-x
Sheibani A, Shishehbor MR, Alaei H (2012) Removal of Fe (III) ions from aqueous solution by hazelnut hull as an adsorbent. Int J Ind Chem 3:4. https://doi.org/10.1186/2228-5547-3-4
Simonin J-P, Bouté J (2016) Intraparticle diffusion-adsorption model to describe liquid/solid adsorption kinetics. Revista Mexicana De Ingeniería Química 15:161–173
Soylak M, Unsal YE, Kizil N, Aydin A (2010) Utilization of membrane filtration for preconcentration and determination of Cu(II) and Pb(II) in food, water and geological samples by atomic absorption spectrometry. Food Chem Toxicol 48:517–521. https://doi.org/10.1016/j.fct.2009.11.005
Sun M, Nelson AE, Adjaye J (2006) Examination of spinel and nonspinel structural models for γ-Al2O3 by DFT and rietveld refinement simulations. J Phys Chem B 110(5):2310–2317

Wahid F, Wang H-S, Lu Y-S, Zhong C, Chu L-Q (2017) Preparation, characterization and antibacterial applications of carboxymethyl chitosan/CuO nanocomposite hydrogels. Int J Biol Macromol 101:690–695. https://doi.org/10.1016/j.ijbiomac.2017.03.13

Wang J, Guo X (2020) Adsorption kinetic models: physical meanings, applications, and solving methods. J Hazard Mater 390:122156. https://doi.org/10.1016/j.jhazmat.2020.122156

Wang H, Shadman F (2012) Effect of particle size on the adsorption and desorption properties of oxide nanoparticles. AIChE J 59(5):1502–1510. https://doi.org/10.1002/aic.13936

Yao W, Weng Y, Catchmark JM (2020) Improved cellulose X-ray diffraction analysis using fourier series modeling. Cellulose 27(10):5563–5579. https://doi.org/10.1007/s10570-020-03177-8

Yeddou N, Bensmaili A (2007) Equilibrium and kinetic modelling of iron adsorption by eggshells in a batch system: effect of temperature. Desalination 206(1–3):127–134. https://doi.org/10.1016/j.desal.2006.04.052

Yuan Y, Zhang G, Li Y, Zhang G, Zhang F, Fan X (2013) Poly(amidoamine) modified graphene oxide as an efficient adsorbent for heavy metal ions. Polym Chem 4:2164–2167. https://doi.org/10.1039/C3PY21128B

Zhang H, Chen L, Zhang LP, Yu XJ (2010) Impact of environmental conditions on the adsorption behavior of radionuclide Ni(II) onto hematite. J Radioanal Nucl Chem 287:357–365. https://doi.org/10.1007/s10967-010-0686-2

Zhang W, Liu Y, Xuan Y, Zhang S (2022) Synthesis and applications of carboxymethyl cellulose hydrogels. Gels 8:529. https://doi.org/10.3390/gels8090529

Zuo C, Li Q, PENG G, Xing G, (2011) Manufacture of biomorphic Al2O3 ceramics using filter paper as template. Progress Nat Sci Mater Int 21(6):455–459. https://doi.org/10.1016/s1002-0071(12)60082-3